Nonlinear steady convection in rotating mushy layers

D. N. Riahi

Department of Theoretical and Applied Mechanics

216 Talbot Laboratory, 104 South Wright Street

University of Illinois at Urbana-Champaign

Urbana, Illinois 61801 U. S. A.

Abstract

We consider the problem of nonlinear steady convection in a horizontal mushy layer rotating about a vertical axis. We analyze the stationary modes of convection in the form of two-dimensional oblique rolls and three-dimensional distorted patterns. Under a near-eutectic approximation and the limit of large far-field temperature, we determine the two- and three-dimensional solutions to the weakly nonlinear problem by using a perturbation technique, and the stability of these solutions are investigated with respect to arbitrary three-dimensional disturbances. The results of the analyses in particular range of values of the amplitude of convection indicate, in particular, that, over most of the range of values of the parameters, subcritical convection in the form of down-hexagons with down-flow at the cells' centers and up-flow at the cells' boundaries can be preferred over the up-hexagonal convection, where the convective flow is upward at the cells' centers and downward at the cells' boundaries. For zero or very small values of T ($T \ll 1$), which is the square root of a Taylor number, rolls are preferred over the supercritical rectangles, while supercritical rectangles, which are characterized by an angle γ about 60°, are stable and preferred over the rolls for T above some value. Here, γ or 180°-γ are the angles

between any two adjacent wave number vectors of a rectangle cell. For increasing values of T, these rectangles become subcritically unstable and are replaced by new supercritical rectangles of higher γ values, and γ increases with T until supercritical squares (γ=90°) become stable. The significance and realizability of down-hexagons, rectangles and squares are found to be due to the interactions between the local solid fraction and the flow associated with the Coriolis term in the momentum-Darcy equation that are fully taken into account in the present study.

1. Introduction

Recently Guba (2001) considered the problem of finite-amplitude steady convection in a horizontal mushy layer rotating about a vertical axis. The investigation was based on the mushy-layer model developed by Amberg and Homsy (1993) and Anderson and Worster (1995) where a near –eutectic approximation was employed in the limit of large far-field temperature. The model allows examination of the dynamics of the mushy layer in the form of small deviation from the classical system of convection in a horizontal porous layer of constant permeability. Guba (2001) did not take into account the presence of the interactions between the local solid fraction and the convection associated with the Coriolis term in the Darcy-momentum equation by fixing the local solid fraction at a constant value in the term modeling the effect of rotation. The goal of the author was, then, to determine how rotation of the system affects the convection in such a relatively simple case in the absence of those interaction effects. In addition, the author assumed that the amplitude of convection is of the same order as the thickness of the mushy layer. The form of the finite-amplitude convection studied by Guba (2001) was that due to either two-dimensional oblique rolls or distorted hexagons. As the author

explained and more details can be found in Veronis (1959), due to the rotation of the system, the two-dimensional rolls are oblique in the sense that the streamlines of the flow are confined to the planes, which are in the directions at oblique angles to the axes of convection rolls. Similarly, the hexagonal patterns are distorted in the presence of rotation. Guba (2001) found, in particular, that depending on the range of the parameter values, either subcritical or supercritical oblique rolls can exist and the distorted subcritical hexagons can change their form from up-hexagons to down-hexagons for the rotation rate beyond some critical value.

In the present investigation, we extend the problem treated by Guba (2001) by following Anderson and Worster (1995) in assuming a much wider range of values for the amplitude of convection, taking into account the presence of the interactions between the local solid fraction and the convection associated with the Coriolis term in the momentum-Darcy equation and carrying out stability analysis of the finite-amplitude steady solutions. We found a number of interesting results some of which sharply differ from those obtained based on a model of the type studied by Guba (2001). The differences between some the results in the present study and those due to Guba (2001) are discussed in some details in section 5. It should be noted that to appreciate the results of the present study, which is based on a more realistic model, we also carried out some calculations based on the model of the type studied by Guba (2001). We found, for example, that for the model of the type due to Guba (2001), convection in the form of rectangles and squares is not stable and, thus, not preferred over the rolls, while in the present model convection in the form of supecritical rectangles or supercritical squares can be stable and preferred over the rolls in particular range of values of the rotation rate.

However, subcritical rectangles or subcritical squares, which can exist in particular range of values of the rotation rate, are found to be unstable.

In regard to the motivation of the present study and the applicability of the present results, it should be noted that understanding the rotational effects on the buoyancy driven convection in a mushy layer, which is formed adjacent to the crystal interface in an alloy system, are of interest in both engineering and geophysical areas. Understanding the roles and effects of the Coriolis force on the dynamics of a possible mushy layer adjacent to the earth's inner core interface can be important for further understanding the geodynamo. In industrial crystal growth processes it has been desirable to impose certain external constraints such as rotation, in an optimized manner upon the crystallization system, in order to reduce the effects of the induced convection flow, which can lead to micro-defect density in the crystal and, thus, reduce the quality of the produced crystal. Some theoretical results on the effects of rotation about a vertical axis on the flow of melt during alloy solidification and in the absence of a mushy layer (Riahi1993) indicated conditions under which rotation may stabilize the flow. Computational studies on the effects of rotation about a vertical axis of a horizontal layer on the flow of melt during alloy solidification (Neilson and Incropera1993) indicated stabilization of vertical plumes and their lack of meandering due to such a rotational constraint. The occurrences of undesirable imperfections, which are called freckles, in the alloy crystal, are believed to be due to convection in vertical chimneys, which are developed beyond the onset of the plume convection within the mushy layer. In the present study we are interested to determine the effects of rotation on the onset of plume convection, tendency for chimney

formation and the finite-amplitude steady convection states, which realize near the onset of motion.

The following two sections 2-3 deal with the mathematical formulation of the problem and the finite-amplitude analysis. The results of the steady solutions are presented and discussed in section 4, which is followed by the conclusion and some remarks in section 5.

2. Formulation

We consider a binary alloy melt that is cooled from below and is solidified at a constant speed V_0. Following Amberg and Homsy (1993) and Anderson and Worster (1995), we consider a mushy layer of thickness d adjacent and above the solidification front to be physically isolated from the overlying liquid and the underlying solid zones. The overlying liquid is assumed to have a composition $C_0 > C_e$ and temperature $T_\infty > T_L(C_0)$ far above the mushy layer, where C_e is the eutectic composition, $T_L(\tilde{C})$ is the liquidus temperature of the alloy and $\tilde{C}$ is the composition. It is then assumed that the horizontal mushy layer is bounded from above and below by rigid and isothermal boundaries. The solidifying system is assumed to be rotating at a constant speed ω in the vertical direction anti-parallel to the gravity vector. We consider the solidifying system in a moving frame of reference $o\tilde{x}\tilde{y}\tilde{z}$, whose origin lies on the solidification front, translating at the speed V_0 with the solidification front in the positive $\tilde{z}$-direction and rotating with the speed ω along the $\tilde{z}$-axis.

It should be noted that no double-diffusive effect is present in the above described one-layer mushy zone model since such a mushy layer is assumed to be in local thermodynamic equilibrium and, thus,

$$\tilde{T}=T_L(C_0)+\Gamma(\tilde{C}-C_0),$$

where $\tilde{T}$ is the temperature and Γ is the slope of the liquidus (Anderson and Worster1995), which is assumed to be constant. The mushy layer is treated appropriately as a porous layer (Fowler1985; Worster1992), where the solid dendrites and the liquid coexist, and Darcy's law is adopted.

Next, we consider the equations for momentum, continuity, heat and solute for the flow of melt in the mushy layer in the already described moving frame. These equations are non-dimensionalized by using V_0, k/V_0, k/V_0^2, $\beta\Delta C\ \rho gk/V_0$, ΔC and ΔT as scales for velocity, length, time, pressure, solute and temperature, respectively. Here k is the thermal diffusivity, ρ is a reference (constant) density, $\beta=\beta^*-\Gamma\alpha^*$, where α^* and β^* are the expansion coefficients for the heat and solute, respectively, $\Delta C=C_0-C_e$, $\Delta T=T_L(C_0)-T_e$ and T_e is the eutectic temperature. The non-dimensional form of the equations for momentum, continuity, temperature and solute concentration in the mushy layer are

$$K(\tilde{\phi})\tilde{\mathbf{u}}=-\nabla\tilde{P}-\tilde{R}\,\tilde{\theta}\mathbf{z}+T\tilde{\mathbf{u}}\times\mathbf{z}/(1-\tilde{\phi}), \tag{1a}$$

$$\nabla.\tilde{\mathbf{u}}=0, \tag{1b}$$

$$(\partial/\partial\tilde{t}-\partial/\partial\tilde{z})(\tilde{\theta}-S_t\tilde{\phi})+\tilde{\mathbf{u}}.\nabla\tilde{\theta}=\nabla^2\tilde{\theta}, \tag{1c}$$

$$(\partial/\partial\tilde{t}-\partial/\partial\tilde{z})[(1-\tilde{\phi})\theta+C_r\tilde{\phi}]+\tilde{\mathbf{u}}.\nabla\tilde{\theta}=0, \tag{1d}$$

where $\tilde{\mathbf{u}}=\tilde{u}\mathbf{x}+\tilde{v}\mathbf{y}+\tilde{w}\mathbf{z}$ is the volume flux vector per unit area, which is also known as Darcy velocity vector (Nield1998), $\tilde{u}$ and $\tilde{v}$ are the horizontal components of $\tilde{\mathbf{u}}$ along $\tilde{x}$- and $\tilde{y}$-directions, respectively, $\mathbf{x}$ and $\mathbf{y}$ are unit vectors along the positive $\tilde{x}$- and $\tilde{y}$-

formation and the finite-amplitude steady convection states, which realize near the onset of motion.

The following two sections 2-3 deal with the mathematical formulation of the problem and the finite-amplitude analysis. The results of the steady solutions are presented and discussed in section 4, which is followed by the conclusion and some remarks in section 5.

2. Formulation

We consider a binary alloy melt that is cooled from below and is solidified at a constant speed V_0. Following Amberg and Homsy (1993) and Anderson and Worster (1995), we consider a mushy layer of thickness d adjacent and above the solidification front to be physically isolated from the overlying liquid and the underlying solid zones. The overlying liquid is assumed to have a composition $C_0 > C_e$ and temperature $T_\infty > T_L(C_0)$ far above the mushy layer, where C_e is the eutectic composition, $T_L(\tilde{C})$ is the liquidus temperature of the alloy and $\tilde{C}$ is the composition. It is then assumed that the horizontal mushy layer is bounded from above and below by rigid and isothermal boundaries. The solidifying system is assumed to be rotating at a constant speed ω in the vertical direction anti-parallel to the gravity vector. We consider the solidifying system in a moving frame of reference $o\tilde{x}\tilde{y}\tilde{z}$, whose origin lies on the solidification front, translating at the speed V_0 with the solidification front in the positive $\tilde{z}$-direction and rotating with the speed ω along the $\tilde{z}$-axis.

It should be noted that no double-diffusive effect is present in the above described one-layer mushy zone model since such a mushy layer is assumed to be in local thermodynamic equilibrium and, thus,

$$\tilde{T}=T_L(C_0)+\Gamma(\tilde{C}-C_0),$$

where $\tilde{T}$ is the temperature and Γ is the slope of the liquidus (Anderson and Worster1995), which is assumed to be constant. The mushy layer is treated appropriately as a porous layer (Fowler1985; Worster1992), where the solid dendrites and the liquid coexist, and Darcy's law is adopted.

Next, we consider the equations for momentum, continuity, heat and solute for the flow of melt in the mushy layer in the already described moving frame. These equations are non-dimensionalized by using V_0, k/V_0, k/V_0^2, $\beta\Delta C\ \rho gk/V_0$, ΔC and ΔT as scales for velocity, length, time, pressure, solute and temperature, respectively. Here k is the thermal diffusivity, ρ is a reference (constant) density, $\beta=\beta^*-\Gamma\alpha^*$, where α^* and β^* are the expansion coefficients for the heat and solute, respectively, $\Delta C=C_0-C_e$, $\Delta T=T_L(C_0)-T_e$ and T_e is the eutectic temperature. The non-dimensional form of the equations for momentum, continuity, temperature and solute concentration in the mushy layer are

$$K(\tilde{\phi})\tilde{\mathbf{u}}=-\nabla\tilde{P}-\tilde{R}\,\tilde{\theta}\mathbf{z}+T\tilde{\mathbf{u}}\times\mathbf{z}/(1-\tilde{\phi}), \tag{1a}$$

$$\nabla.\tilde{\mathbf{u}}=0, \tag{1b}$$

$$(\partial/\partial\,\tilde{t}-\partial/\partial\tilde{z})(\tilde{\theta}-S_t\tilde{\phi})+\tilde{\mathbf{u}}.\nabla\tilde{\theta}=\nabla^2\tilde{\theta}, \tag{1c}$$

$$(\partial/\partial\,\tilde{t}-\partial/\partial\,\tilde{z}\,)[(1-\tilde{\phi})\theta+C_r\tilde{\phi}]+\tilde{\mathbf{u}}\,.\nabla\tilde{\theta}=0, \tag{1d}$$

where $\tilde{\mathbf{u}}=\tilde{u}\mathbf{x}+\tilde{v}\mathbf{y}+\tilde{w}\mathbf{z}$ is the volume flux vector per unit area, which is also known as Darcy velocity vector (Nield1998), $\tilde{u}$ and $\tilde{v}$ are the horizontal components of $\tilde{\mathbf{u}}$ along $\tilde{x}$- and $\tilde{y}$-directions, respectively, $\mathbf{x}$ and $\mathbf{y}$ are unit vectors along the positive $\tilde{x}$- and $\tilde{y}$-

directions, $\tilde{w}$ is the vertical component of $\tilde{\mathbf{u}}$ along $\tilde{z}$-direction, $\mathbf{z}$ is a unit vector along the positive $\tilde{z}$-direction, $\tilde{P}$ is the modified pressure, $\tilde{\theta}$ is the non-dimensional composition, or equivalently temperature (Worster1992), $\tilde{\theta}=[\tilde{T}-T_L(C_0)]/\Delta T=(\tilde{C}-C_0)/\Delta C$, $\tilde{t}$ is the time variable, $\tilde{\phi}$ is the local solid fraction, $\tilde{R}=\beta\Delta C g\,\Pi(0)/(V_0\nu)$ is the Rayleigh number, $\Pi(0)$ is reference value at $\tilde{\phi}=0$ of the permeability $\Pi(\tilde{\phi})$ of the porous medium, which is assumed to be finite (Worster1992), ν is the kinematic viscosity, g is acceleration due to gravity, $K(\tilde{\phi})\equiv\Pi(0)/\Pi(\tilde{\phi})$, $S_t=L/(C_L\Delta T)$ is the Stefan number, C_L is the specific heat per unit volume, L is the latent heat of solidification per unit volume, $C_r=(C_s-C_0)/\Delta C$ is a concentration ratio, C_s is the composition of the solid-phase forming the dendrites and $T=2\omega\Pi(0)/\nu$ is the Coriolis parameter, which is the square root of a Taylor number. The equation (1d) is based on the limit of sufficiently large value of the Lewis number k/k_s (Worster1992; Anderson and Worster1995), where k_s is the solute diffusivity.

The governing equations (1a)-(1d) are subject to the following boundary conditions (Amberg and Homsy1993):

$$\tilde{\theta}+1=\tilde{w}=0 \quad \text{at } \tilde{z}=0, \tag{2a}$$

$$\tilde{\theta}=\tilde{w}=\tilde{\phi}=0 \quad \text{at } \tilde{z}=\delta, \tag{2b}$$

where $\delta=dV_0/k$ is a growth Peclet number representing the dimensionless depth of the layer.

Following Amberg and Homsy and Anderson and Worster (1995) in reducing the model asymptotically, we assume the following rescaling in the limit of sufficiently small δ:

$$C_r=C/\delta,\ \varepsilon<<\delta<<1, \tag{3a}$$

$$(\tilde{x},\tilde{y},\tilde{z})=(x,y,z)\delta\,,\ \tilde{t}=\delta^2 t,\ R^2=\delta\tilde{R}, \tag{3b}$$

$$\tilde{\theta} = \theta_B(z) + \varepsilon\theta(x, y, z, t), \tag{3c}$$

$$\tilde{\phi} = \phi_B(z) + \varepsilon\phi(x, y, z, t), \tag{3d}$$

$$\tilde{\mathbf{u}} = 0 + (\varepsilon R/\delta)\mathbf{u}(x, y, z, t), \tag{3e}$$

$$\tilde{P} = RP_B(z) + R\varepsilon P(x, y, z, t), \tag{3f}$$

where C is an order one quantity as $\delta \to 0$, and the quantities with subscript 'B' are the basic flow variables for the motionless state and are assumed to be a function of z only. The small deviation of each dependent variable from its basic quantity is measured by a perturbation amplitude ε and can vary with respect to spatial and time variables as shown in (3c)-(3f).

As discussed in Anderson and Worster (1995), the assumption of thin mushy layer ($\delta << 1$) is associated with large non-dimensional far-field temperature $\theta_\infty = [T_\infty - T_L(C_0)]/\Delta T >> 1$, which can occur when the initial $\tilde{C}$ is close to C_e. The assumption of order one quantity C corresponds to the near-eutectic approximation (Fowler1985), which allows one to describe the mushy layer as a porous layer of constant permeability to the leading order.

The rescaling (3a)-(3f) are then used in (1a)-(1d) and (2a)-(2b). This system of equations and boundary conditions admits a motionless basic state, which is steady and horizontally uniform. The basic state solution is given below in terms of the asymptotic expansions for $\delta << 1$:

$$\theta_B = (z-1) + \delta(z - z^2)/2 + \ldots, \tag{4a}$$

$$\phi_B = \delta(1-z)/C + \delta^2[-(1-z)^2/C^2 + (z^2 - z)/(2C)] + \ldots, \tag{4b}$$

$$P_B = P_0 + R[(z - z^2/2) + \delta(z^2/2 - z^3/3)/2 + \ldots], \tag{4c}$$

where P_0 is a constant. Since $\tilde{\phi}$ is expected to be small, according to (4b), the following expansion for $K(\tilde{\phi})$ will be implemented later in the governing system:

$$K(\tilde{\phi})=1+K_1\tilde{\phi}+K_2\tilde{\phi}^2+..., \tag{5}$$

where K_1 and K_2 are constants (Amberg and Homsy1993).

For the analysis to be presented in the next section, it is convenient to use the general representation

$$\mathbf{u}=\Omega V+E\psi, \tag{6a}$$

$$\Omega\equiv\nabla\times\nabla\times\mathbf{z},\ \ E\equiv\nabla\times\mathbf{z}, \tag{6b}$$

for the divergent-free vector field $\mathbf{u}$ (Chandrasekhar1961). Here V and ψ are the poloidal and toroidal functions for $\mathbf{u}$, respectively. Taking the vertical components of the curl and double curl of (1a) and using (1b) in (1)-(2), we find the following system which will be analyzed in the next section

$$\nabla^2[K(\phi_B+\varepsilon\phi)\Delta_2 V]+(\partial/\partial z)[\Omega V.\nabla K(\phi_B+\varepsilon\phi)]+(\partial/\partial z)\{[\nabla K(\phi_B+\varepsilon\phi)\times\nabla\psi].\mathbf{z}\}-R\Delta_2\theta+$$

$$T(\partial/\partial z)\{[1/(1-\phi_B-\varepsilon\phi)]\Delta_2\psi+[\nabla(\partial/\partial z)V\times\nabla(1/(1-\phi_B-\varepsilon\phi))].\mathbf{z}+\nabla_2\psi.\nabla_2(1/(1-\phi_B-\varepsilon\phi))\}=0, \tag{7a}$$

$$K(\phi_B+\varepsilon\phi)\Delta_2\psi+[\nabla(\partial/\partial z)V\times\nabla K(\phi_B+\varepsilon\phi)].\mathbf{z}+\nabla_2\psi.\nabla_2 K(\phi_B+\varepsilon\phi)-T\{[1/(1-\phi_B-\varepsilon\phi)]\Delta_2(\partial/\partial z)V-$$

$$[\nabla\psi\times\nabla(1/(1-\phi_B-\varepsilon\phi))].\mathbf{z}+\nabla_2(\partial/\partial z)V.\nabla_2[1/(1-\phi_B-\varepsilon\phi)]\}=0, \tag{7b}$$

$$(\partial/\partial t-\delta\partial/\partial z)(-\theta+S_t\phi)+R(d\theta_B/dz)\Delta_2 V+\nabla^2\theta=\varepsilon R(\Omega V+E\psi).\nabla\theta, \tag{7c}$$

$$(\partial/\partial t-\partial/\partial z)[(-1+\phi_B)\theta+\theta_B\phi+\varepsilon\phi\theta-C\phi/\delta]+R(d\theta_B/dz)\Delta_2 V=\varepsilon R(\Omega V+E\psi).\nabla\theta, \tag{7d}$$

$$\theta=V=0 \quad \text{at } z=0, \tag{7e}$$

$$\theta=V=\phi=0 \quad \text{at } z=1, \tag{7f}$$

where

$$\Delta_2\equiv\partial^2/\partial x^2+\partial^2/\partial y^2,\ \nabla_2\equiv(\partial/\partial x,\ \partial/\partial y).$$

3. Analysis

In this section we seek steady-state solutions of the nonlinear system (7a)-(7f) by applying a weakly nonlinear analysis, based on a double series expansions in powers of two small parameters for the perturbation quantities, of the type carried out by Busse (1967) and Busse and Riahi (1980). Here the small parameters are δ and ε, which satisfy the condition given in (3a). Following Anderson and Worster (1995), we first make a formal asymptotic expansion in ε and then at each order in ε make a formal asymptotic expansion in δ. The appropriate expansions are for the dependent variables of the perturbation system and for R. These expansions are given below

$$(V, \psi, \theta, \phi, R)=[(V_{00}+\delta V_{01}+...), (\psi_{00}+\delta\psi_{01}+...), (\theta_{00}+\delta\theta_{01}+...), (\phi_{00}+\delta\phi_{01}+...), (R_{00}+\delta R_{01}+...)]+\varepsilon[(V_{10}+\delta V_{11}+...), (\psi_{10}+\delta\psi_{11}+...), (\theta_{10}+\delta\theta_{11}+...), (\phi_{10}+\delta\phi_{11}+...), (R_{10}+\delta R_{11}+...)]+\varepsilon^2[(V_{20}+\delta V_{21}+...), (\psi_{20}+\delta\psi_{21}+...), (\theta_{20}+\delta\theta_{21}+...), (\phi_{20}+\delta\phi_{21}+...), (R_{20}+\delta R_{21}+...)]+... \quad (8)$$

3.1. Linear prooblem

Upon inserting (8) into (7a)-(7f) and disregarding the nonlinear terms, we find the linear problem. At order $\varepsilon^0\delta^0$ the system (7a)-(7f) yield the following results:

$$V_{00}=[(\pi^2+a^2)/(R_{00}a^2)]\sin(\pi z)\sum_{n=-N}^{N} A_n W_n, \quad (9a)$$

$$\psi_{00}=T\pi[(\pi^2+a^2)/(R_{00}a^2)]\cos(\pi z)\sum_{n=-N}^{N} A_n W_n, \quad (9b)$$

$$\theta_{00}= -\sin(\pi z)\sum_{n=-N}^{N} A_n W_n, \quad (9c)$$

$$\phi_{00}=[-(\pi^2+a^2)/(C\pi)][1+\cos(\pi z)]\sum_{n=-N}^{N} A_n W_n, \quad (9d)$$

$$R_{00}^2=(\pi^2+a^2)(\pi^2+a^2+\pi^2 T^2)/a^2, \quad (9e)$$

where

$$W_n=\exp(i\mathbf{a}_n.\mathbf{r}). \tag{9f}$$

Here i is the pure imaginary number (i= -1), subscript 'n' takes only non-zero integer values from –N to N, N is a positive integer representing the number of distinct modes, $\mathbf{r}$ is the position vector, and the horizontal wave number vectors $\mathbf{a}_n$ satisfy the properties

$$\mathbf{a}_n.\mathbf{z}=0,\ |\mathbf{a}_n|=a,\ \mathbf{a}_{-n}=-\mathbf{a}_n. \tag{10}$$

The coefficients A_n are constants and satisfy the conditions

$$\sum_{n=-N}^{N} A_n A_n^*=1,\quad A_n^*=A_{-n}, \tag{11}$$

where the asterisk indicates the complex conjugate. Minimizing the expression for R_{00} given in (9e), with respect to the wave number a, we find

$$R_{00c}=\pi[1+(1+T^2)^{0.5}], \tag{12a}$$

$$a_c=\pi(1+T^2)^{0.25}. \tag{12b}$$

Here R_{00c} is the minimum value of R_{00} achieved at $a=a_c$. In all the analyses and solutions to follow, hereafter, we shall set $R_{00}=R_{00c}$ and $a=a_c$, unless indicated otherwise. As the results to be discussed in the next section indicate, some of the presumed order one coefficients R_{nm} can become too large for T somewhat bigger that 1, and so the validity of the present model may become questionable for large values of T. Hence, we shall assume that the value of T can be at most about 1 or so. Also, due to the complexity of the present rotating flow investigation, which is amplified by taking into account the local solid fraction interaction with the Coriolis term, we consider a simplifying assumption by following Anderson and Worster (1995) and focusing on a particular limiting case where K_1 is small of order δ, so that we can write $K_1=\delta K_c$, where K_c is a constant of order one.

Considering the governing system (7a)-(7f) in the order $\varepsilon^0\delta^1$, eliminating ψ_{01} between (7a) and (7b), multiplying the resulting equation by aV_{00} and (7c) by θ_{00}, adding these

two later equations, averaging over the fluid layer and making use of (7e)-(7f), we find the condition for the existence of the solutions V_{01} and θ_{01}. This condition yield

$$R_{01}=[\pi^2T^2(\pi^2+a^2)/(2Ca^2R_{00})]-R_{00}S_t/(2C) \tag{13a}$$

and at the critical onset condition

$$R_{01c}=[1/(2C)]\{[\pi T^2/(1+T^2)^{0.5}]-\pi[1+(1+T^2)^{0.5}]S_t\}. \tag{13b}$$

Hence, the critical Rayleigh number R_c for the linear system can be written as

$$R_c=R_{00c}+\delta R_{01c}+O(\delta^2). \tag{14}$$

The solutions in this order can be written in the form

$$(V_{01},\psi_{01},\theta_{01},\phi_{01})=[V_{01}^*(z),\psi_{01}^*(z),\theta_{01}^*(z),\phi_{01}^*(z)]\Sigma_{n=-N}^{N} A_nW_n, \tag{15}$$

where the expressions for the coefficients V_{01}^*,ψ_{01}^*,θ_{01}^* and ϕ_{01}^*, which are functions of z and the non-dimensional parameters of the problem, are given in appendix A.

3.2. Nonlinear problem

Next, we analyze the nonlinear problem for the steady convection. The solvability conditions for the nonlinear systems require the following special solutions V_{00n} and θ_{00n} of the linear system:

$$(V_{00n}, \theta_{00n})=[(\pi^2+a^2)/(R_{00}a^2), -1]\sin(\pi z)A_n W_n. \tag{16}$$

It turns out that there is no need to consider special linear solution for ψ and ϕ since the governing nonlinear systems are usually reduced to a form where only (16) will be needed to form the corresponding solvability conditions. Consider the system (7a)-(7f) in order ε. Multiplying the equation, resulted from eliminating ψ_{10} between (7a) and (7b), by $-V_{00n}$, (7c) by θ_{00n}, adding, averaging over the fluid layer and applying the boundary conditions (7e)-(7f), we find

$$R_{10}|A_n|^2=-\pi T^2[(\pi^2+a^2)^2/(CR_{00}a^2)]\Sigma_{l,p}(1+\Phi_{lp})A_n A_l A_p \langle W_n W_l W_p \rangle, \tag{17a}$$

where

$$\Phi_{lp}=\mathbf{a}_l.\mathbf{a}_p\,/a^2, \tag{17b}$$

and an angular bracket indicates the average over the layer. The right-hand-side in (16a) for R_{10} indicates that $R_{10}=0$, unless

$$\mathbf{a}_n+\mathbf{a}_l+\mathbf{a}_p=0 \tag{18}$$

for at least some l and p. The condition (18) can be satisfied in the cases where convection is in the form of either hexagonal or triangular patterns (Busse1989), while (18) can not be satisfied for convection in the form of two-dimensional rolls or squares. It should also be noted that the existence of triangle type solution (N=3) is ruled out in the present problem since a pure imaginary value for A_n, which holds in this case (Gorko1957), does not satisfy (17a). The solutions in this order can be written in the form

$$(V_{10}, \psi_{10}, \theta_{10}, \phi_{10})=[V_{10}^*(z), \psi_{10}^*(z), \theta_{10}^*(z), \phi_{10}^*(z)]\sum_{n=-N}^{N} A_n W_n +\sum_{l,p} [V_{10}\hat{}(z,\Phi_{lp}), \psi_{10}\hat{}(z,\Phi_{lp}), \theta_{10}\hat{}(z,\Phi_{lp}), \phi_{10}\hat{}(z,\Phi_{lp})]\sum_{l,p} A_l A_p W_l W_p\,, \tag{19}$$

where the expressions for V_{10}^*, ψ_{10}^*, θ_{10}^*, ϕ_{10}^*, $V_{10}\hat{}$, $\psi_{10}\hat{}$, $\theta_{10}\hat{}$ and $\phi_{10}\hat{}$ are given in the appendix A.

We also carry out here the analysis for the system (7a)-(7f) in the order $\varepsilon\delta$ mainly due to the result that the magnitude of R_{10} due to (17a) for the hexagonal patterns is found to be rather small in the range of T that is considered in the present study. Consider the system (7a)-(7f) in the order $\varepsilon\delta$. Multiplying the equation, resulted from eliminating ψ_{11} between (7a) and (7b), by $-V_{00n}$, (7c) by θ_{00n}, adding, averaging over the fluid layer and applying the boundary conditions (7e)-(7f), we find

$$R_{11}|A_n|^2 =\sum_{l,p} F_{11}(\Phi_{lp})A_n A_l A_p \langle W_n W_l W_p\rangle+G_{11}|A_n|^2, \tag{20}$$

where the expressions for the coefficients F_{11} and G_{11} are given in the appendix A. As in the case of R_{10}, $R_{11}=0$, unless (18) holds for at least some l and p since the expression for G_{11} is zero for $R_{10}=0$ and the summation term in the right-hand-side of (20) vanishes if (18) does not hold. The solutions in this order are quite lengthy and will not be given in this paper.

We now consider the system (7a)-(7f) in order ε^2. Multiplying the equation, resulted from eliminating ψ_{20} between (7a) and (7b), by $-V_{00n}$, (7c) by θ_{00n}, adding, averaging over the fluid layer and applying the boundary conditions (7e)-(7f), we find

$$R_{20}|A_n|^2= \sum_{l,m,p} F_{20}(\Phi_{lp}, \Phi_{ml}, \Phi_{mp})A_n A_l A_m A_p <W_n W_l W_m W_p>+ \sum_{l,p} H_{20}(\Phi_{lp})A_n A_l A_p <W_n W_l W_p>+G_{20}|A_n|^2, \quad (n=-N, ..., -1, 1, ..., N), \tag{21}$$

where the summations in (21) for l, m and p run from –N to N, and the expressions for F_{20}, H_{20} and G_{20} are given in the appendix A.

The system (21) contains integral expressions of the form $<W_n W_l W_p>$, which differ from zero only if (18) is satisfied, and integral expressions of the form $<W_n W_l W_m W_p>$, which differ from zero only if

$$\mathbf{a}_n +\mathbf{a}_l +\mathbf{a}_m +\mathbf{a}_p=0. \tag{22}$$

The system (21), together with (11), (17a) and (20), can be used to study the steady solutions in the form of two-dimensional oblique rolls and three-dimensional distorted cells. We shall restrict our attention to the simplest types of solutions, which include those observed in the applications. These solutions are called regular or semi-regular solutions (Busse1967). In the case of a regular solution all angles between two neighboring **a**-vectors are equal and (11) yield

$$|A_1|^2=...=|A_N|^2=1/(2N). \tag{23}$$

In the more general semi-regular solution, where (23) still holds, the scalar products between any of the **a**-vectors and its two neighboring **a**-vectors assume the constant values α_1 and α_2. An example of a semi-regular solution is that due to rectangular cells (N=2), where $\alpha_1 = -\alpha_2$. Regular solutions can follow from the semi-regular ones for the special case $\alpha_1 = \alpha_2$. Simple forms of regular solutions correspond to the cases of two-dimensional rolls (N=1), square cells (N=2) and hexagons (N=3).

Thus, using (11), (18) and (22)-(23) in (17a), (20) and (21), we find

$$R_{10} = [-\pi T^2(\pi^2+a^2)^2/(CR_{00}a^2\sqrt{6})]S, \tag{24a}$$

$$R_{11} = [2F_{11}(\Phi_{lp}=0.5)/\sqrt{6} + G_{11}]S, \tag{24b}$$

$$R_{20} = \sum_{m=-N}^{N} T_{nm}|A_m|^2 + (2/\sqrt{6})H_{20}(\Phi_{lp}=0.5)S + G_{20}, \quad (n=-N, ..., -1, 1, ..., N), \tag{24c}$$

where

$$S=1 \text{ for hexagons and } 0 \text{ for non-hexagons,} \tag{24d}$$

$$T_{nm} = F_{-n,n,-n}\,\delta_{nm} + (F_{n,-n,-n}+F_{-n,-n,n})\delta_{n,-m} + (F_{-m,m-n}+F_{-n,m,-m}+F_{m,-n,-m})(1-\delta_{nm})(1-\delta_{n,-m}),\ F_{l,m,p} \equiv F_{20}(\Phi_{lp}, \Phi_{ml}, \Phi_{mp}), \tag{24e}$$

$$\delta_{nm}=1 \text{ for } n=m \text{ and } 0 \text{ for } n \neq m. \tag{24f}$$

Here by the term 'non-hexagons' in (24d) it is meant solution whose wave number vectors do not contain a sub-set of such vectors, which can satisfy a condition of the type (18).

The simplest types of solutions, which turn out to be preferred under certain conditions in the present study, are described briefly as follows. For steady two-dimensional oblique rolls, N=1, $A_n=1/\sqrt{2}$ and S=0 in (24). For distorted rectangular pattern convection, N=2, $A_n=1/2$, $\gamma \neq 90°$ and S=0 in (24). Here γ is the angle ($\gamma \leq 90°$) between two adjacent wave number vectors of any cell. For distorted square pattern convection,

N=2, A_n=1/2, γ=90° and S=0 in (24). For distorted up-hexagonal convection, N=3, A_n =1/$\sqrt{6}$, $R_{10}+\delta R_{11}$ <0 and S=1 in (24). For distorted down-hexagonal convection, N=3, A =1/$\sqrt{6}$, $R_{10}+\delta R_{11}$ >0 and S=1 in (24). As will be referred to later in section 4, the sign of the vertical motion at the cells' centers for hexagons, which is determined by the sign of ε, can be inferred from the condition

$$\varepsilon(R_{10}+\delta R_{11})<0 \tag{25}$$

for the preferred subcritical hexagons. As indicated before, the value of R_{10} in the present problem is found to be rather small for the assumed range of values for T, and, thus, the sign of $(R_{10}+\delta R_{11})$ is appropriately taken into account to determine whether hexagons are subcritical or supercritical.

3.3. Stability problem

The analysis of the nonlinear steady convection presented in the previous sub-section has shown that an infinite manifold of solutions could exist even though this manifold represents only an infinitesimal fraction of the manifold of the solutions (9a)-(9d) of the linear problem. To distinguish the physically realizable solution among all the possible steady solutions, the stability of V,ψ, θ, ϕ with respect to arbitrary three-dimensional disturbances V_d, ψ_d, θ_d, ϕ_d need to be investigated. The time-dependent disturbances can be assumed in the form

$$(V_d, \psi_d, \theta_d, \phi_d)=[V'(x, y, z), \psi'(x, y, z), \theta'(x, y, z), \phi'(x, y, z)]\exp(\sigma t), \tag{26}$$

where σ is the growth rate of the disturbances. When the governing equations and the boundary conditions of the form (7a)-(7f) for the finite-amplitude steady flow are subtracted from the corresponding equations and boundary conditions for the total dependent variables for the steady flow and the disturbance quantities and the resulting

system is linearized with respect to the disturbance quantities, we obtain the stability system, which is given by (B1a)-(B1f) in appendix B.

When the expansion (8) is used in (B1a)-(B1f), it becomes evident that the stability system can be solved by a similar expansion

$$(V', \psi', \theta', \phi', \sigma)=[(V'_{00}+\delta V'_{01}+...), (\psi'_{00}+\delta\psi'_{01}+...), (\theta'_{00}+\delta\theta'_{01}+...), (\phi'_{00}+\delta\phi'_{01}+...),$$

$$(\sigma_{00}+\delta\sigma_{01}+...)]+\varepsilon[(V'_{10}+\delta V'_{11}+...), (\psi'_{10}+\delta\psi'_{11}+...), (\theta'_{10}+\delta\theta'_{11}+...), (\phi_{1(-1)}$$

$$/\delta+\phi'_{10}+\delta\phi'_{11}+...), (\sigma_{10}+\delta\sigma_{11}+...)]+\varepsilon^2[(V_{2(-1)}/\delta+V'_{20}+\delta V'_{21}+...), (\psi_{2(-1)}/\delta+\psi'_{20}+\delta\psi'_{21}+...),$$

$$(\theta_{2(-1)}/\delta+\theta'_{20}+\delta\theta'_{21}+...), (\phi_{2(-1)}/\delta+\phi'_{20}+\delta\phi'_{21}+...), (\sigma_{20}+\delta\sigma_{21}+...)]+... , \qquad (27)$$

where the expansions for ϕ' and all the disturbance variables are singular at order ε and ε^2, respectively, as $\delta\rightarrow 0$, but, it turns out, that such $O(1/\delta)$ terms are needed in the stability analysis since it is found that the $O(\varepsilon)$ and $O(\varepsilon^2)$ of the stability problem are forced by terms of order $1/\delta$ in the equations for the disturbances.

For the present stability analysis we restrict ourselves to those disturbances whose dependent variables have wave number vectors $\mathbf{a}'_n$, which all have the same wave number $|\mathbf{a}'_n|= a'=a_c$. Then the most critical disturbances, which have the maximum growth rate, are found to be characterized by $\sigma_0 =0$, where

$$\sigma_0=\sigma_{00}+\delta\sigma_{01}+...$$

The linear solutions for the dependent variables of the disturbances at order δ^0 are found to be of the form (9a)-(9d), provided A_n, W_n and N are replaced by arbitrary constants $\tilde{A}_n$, $\tilde{W}_n = \exp(i\mathbf{a}'_n.\mathbf{r})$ and ∞, respectively.

In analogy to the solvability conditions for the steady motion presented in the previous sub-section, the solvability conditions for the disturbance systems in the order ε (n>1)

require us to define particular solutions of the linear system for the disturbance system. These solutions designated by $\tilde{V}_{00n}$ and $\tilde{\theta}_{00n}$ have the same form as (15), provided A_n and W_n are replaced, respectively, by $\tilde{A}_n$ and $\tilde{W}_n$. The solvability condition for the disturbance system in the order ε is derived similar to the corresponding one for the steady flow system. We first derived the disturbance system at order ε from (B1a)-(B1f). Then we eliminated ψ'_{10} between (B1a) and (B1b) in the order ε. Next, we multiplied the equation, resulted from eliminating ψ'_{10} between (B1a) and (B1b) by $-\tilde{V}_{00n}$, (B1c) by $\tilde{\theta}_{00n}$, added, averaged over the fluid layer and applied the boundary conditions (B1e)-(B1f). We then found the expression for σ_{10}. Similarly, we applied the solvability conditions in the orders $\varepsilon\delta$ and ε^2 to determine σ_{11} and σ_{20}. Since σ_{10}, σ_{11} or σ_{20} may not in general be zero for a particular solution, we define

$$\sigma^* = \varepsilon\sigma_{10} + \varepsilon\delta\sigma_{11} + \varepsilon^2\sigma_{20} \tag{28a}$$

as the leading order growth rate and combine the solvability conditions in the orders ε , $\varepsilon\delta$ and ε^2 to obtain the following system for σ^*:

$$(-\sigma^* M + R^*)|\tilde{A}_n|^2 = \sum_{l,p} [\varepsilon L_{10}(\Phi_{lp}, \Psi_{lp}) + \varepsilon\delta L_{11}(\Phi_{lp}, \Psi_{lp}) + \varepsilon^2 L_{20}(\Phi_{lp}, \Psi_{lp})](\tilde{A}_n \tilde{A}_l A_p \langle \tilde{W}_n \tilde{W}_l W_p \rangle + \tilde{A}_n A_l \tilde{A}_p \langle \tilde{W}_n W_l \tilde{W}_p \rangle) + \sum_{l,m,p} \varepsilon^2 [F_{20}(\Phi_{lp}, \Phi_{ml}, \Phi_{mp}) + \tilde{F}_{20}(\Phi_{lp})(\Psi_{ml} + \Psi_{mp})](\tilde{A}_n \tilde{A}_l A_m A_p \langle \tilde{W}_n \tilde{W}_l W_m W_p \rangle + \tilde{A}_n A_l \tilde{A}_m A_p \langle \tilde{W}_n W_l \tilde{W}_m W_p \rangle + \tilde{A}_n A_l A_m \tilde{A}_p \langle \tilde{W}_n W_l W_m \tilde{W}_p \rangle), \tag{28b}$$

where

$$R^* = \varepsilon R_{10} + \varepsilon\delta(R_{11} - G_{11}) + \varepsilon^2(R_{20} - G_{20}), \tag{28c}$$

$$\Psi_{lp} = [(\mathbf{a}_l \times \mathbf{a}_p).\mathbf{z}]/a^2, \tag{28d}$$

$$M = R_{00}/[2(\pi^2 + a^2)], \tag{28e}$$

and the expressions for $\tilde{F}_{20}$, L_{10}, L_{11} and L_{20} are given in the appendix B. The growth rates σ^* of the disturbances acting on the finite-amplitude steady motion can then be determined from (28) following the method approach due to Busse (1967), which is now a standard stability procedure, for cases where the wave number vectors of the disturbances either coincide with those of the steady motion or not.

4. Results and discussion

4.1. Linear problem

The linear system and its eigenvalue problem, which led to the results (9)-(15), are, in general, functions of the parameters C, S_t and T. Here and thereafter value of δ=0.2 is chosen to evaluate R_c and other quantities whose values may depend on δ. The well known stabilizing effect of the Coriolis force on convection (Chandrasekhar1961) can be seen from the expressions for R_c and a_c, which can be found from (12a)-(12b), (13b) and (14). Both R_c and a_c increase with T. However, a_c is independent of C and S_t, while R_c depends only weakly on these two parameters. For T=0, R_c decreases with increasing S_t, for a given C, and increases with C, for a given S_t. Thus, the effects of increasing S_t and C are, respectively, destabilizing and stabilizing at the onset of motion. These results are understandable with respect to the physical interpretation of the parameters S_t and C since S_t represents a measure of the latent heat relative to the heat content and C represents the difference in the characteristic composition of the solid and liquid phases to the compositional variation of the liquid. However, in the rotating case (T≠0) there is a competition between the stabilizing effects of C and T, which depends on the values of S_t

and T. Since dependence of R_c on C and S_t is through the expression for R_{01c} given in (13b), we find that for $0<S_t<T_{c1}$, where

$$T_{c1}=T^2/[1+T^2+(1+T^2)^{0.5}], \tag{29}$$

then R_c decreases with increasing either C or S_t. For $S_t>T_{c1}$, then R_c increases with C, while it still decreases with increasing S_t. The value of T_{c1} increases with T and reaches 1 as $T\to\infty$. Thus, in a small range for S_t bounded from above by T_{c1}, the only stabilizing effect is due to T, and both C and S_t are destabilizing in the sense that R_c decreases with increasing either C or S_t. To see the main cause for the destabilizing effect of C when S_t is bounded from above by T_{c1}, we consider the expression (13b) for R_{01c} and note that the first term inside the bracket in the right-hand-side, which is independent of S_t, is due to the interaction between the leading term in the basic state of the local solid fraction and the Coriolis term in the momentum-Darcy equation. If this interaction term is not taken into account, then C cannot exhibit the above-described destabilizing effect. We will uncover more surprising results due to the interactions of the local solid fraction with the Coriolis term later in this section.

Due to degeneracy of the linear system, the above described linear results are applicable to both two- and three-dimensional convection cases whose nonlinear results are presented and discussed in the next sub-section.

4.2. Nonlinear problem

Important quantities due to the nonlinear effects are the coefficients

$$R_1=R_{10}+\delta R_{11}+O(\delta) \tag{30}$$

and R_{20}, which are calculated in the present study. As can be seen from the expansions (8), these coefficients represent leading contributions to the change in R required to

obtain finite amplitude ε for a nonlinear solution. In terms of these coefficients the amplitude of convection is of order

$$|\varepsilon|=\{|R_1|\pm[R_1^2+4R_{20}(R-R_c)]^{0.5}\}/(2R_{20}). \qquad (31)$$

As can be seen from (31), there are two expressions for $|\varepsilon|$ corresponding to plus and minus signs in (31), where the expression with plus sign corresponds to the case where R_{20} is positive, while the expression with negative sign corresponds to the case where R_{20} is negative. It should also be noted that in the case of non-zero R_1, which can correspond to the cases where convection is in the form of hexagons, then the expression (31) for $|\varepsilon|$ is provided only for the preferred subcritical convection state where $R<R_c$. In this case the amplitude of convection is largest if the magnitude of R_1 is largest. For $R_1=0$, which can correspond to the cases of two-dimensional rolls, rectangles and square pattern convection, then the sign of R_{20} determines whether the steady solution exists for values of R above or below R_c. For $R_1=0$ and supercritical convection, where $R>R_c$, the amplitude of convection is largest, provided the value of R_{20} is smallest among all the solutions to the nonlinear problem. In the present problem the coefficients R_1 and R_{20} are due to the linear and nonlinear interactions between the local solid fraction and the Coriolis term in the momentum-Darcy equation, the nonlinear convective terms in the temperature equation and the nonlinear interactions between the flow velocity and the non-uniform and nonlinear permeability associated with the perturbation to the basic state solid fraction.

Hexagonal convection

The coefficient R_1, given by (24a)-(24b) and (30), for the hexagonal convection was computed for various values of T, C, S_t, K_c and K_2. It was found that depending on the

range of the values of the parameters, R_1 can be either positive or negative, and, thus, the steady hexagonal convection can be supercitical for

$$\varepsilon R_1 > 0 \tag{32a}$$

and subcritical for

$$\varepsilon R_1 < 0. \tag{32b}$$

For supercritical case, up-hexagons correspond to the case where

$$\varepsilon > 0 \text{ and } R_1 > 0, \tag{32c}$$

while down-hexagons correspond to the case where

$$\varepsilon < 0 \text{ and } R_1 < 0. \tag{32d}$$

For subcritical case, up-hexagons correspond to the case where

$$\varepsilon > 0 \text{ and } R_1 < 0, \tag{32e}$$

while down-hexagons correspond to the case where

$$\varepsilon < 0 \text{ and } R_1 > 0. \tag{32f}$$

Some typical results about the effects of T and K_c are presented in Figure 1 for R_1 versus T for S_t=5.0, C=1.0, K_2=0.0, and for several values of K_c. It is seen from this figure that for $R_1<0$ ($R_1>0$), $|R_1|$ decreases (increases) with either increasing T or decreasing K_c.

Hence, tendency for the preference of down-hexagons increases with T and decreases with increasing K_c. Conversely, tendency for the preference of up-hexagons decreases with increasing T and increases with K_c. Our additional generated data indicated that R_1 is negative for T=0, which agrees with the result due to Amberg and Homsy (1993), but for $T \neq 0$, R_1 increases with T until it becomes zero at a critical T_{c2} of T, beyond which R_1 is positive and generally increases rather rapidly with T. This result was one of the main

reason to restrict the present investigation to the cases of small and at most about 1 values of T. For larger values of T, the values of $|R_1|$ become very large that can invalidate the basic assumption for the expansions of type (8) for the present model. The value of T_{c2} was found to increase with increasing C or with decreasing S_t. In addition to the effect of the scaled linear measure of the permeability variations K_c, our generated data indicated that the effect of a nonlinear measure of the permeability variations K_2 is also to favor up-hexagons in the sense that $|R_1|$ increases with K_2 when $R_1<0$ and decreases with increasing K_2 when $R_1>0$.

Some typical results about variations of R_1 with respect to C and S_t are presented in Figures 2-3 for $K_c=0.1$, $K_2=0.0$ and for several values of T. Figure 2 presents R_1 versus C at $S_t=1.0$ and for T=0.0, 0.25 and 0.50. It is seen from this figure that for T=0, R_1 is negative, $|R_1|$ is small, and the effect of C is stabilizing in the sense that subcritical effect is reduced with increasing C. For $T \neq 0$ and above T_{c2}, R_1, which is large for small values of C, decreases rather rapidly with increasing C until R_1 becomes zero at some critical C_c of C. For $C>C_c$, R_1 is negative and $|R_1|$ increases slowly with C. The value of C_c is found to increase with T. Hence, in the rotating case for $T>T_{c2}$, down-hexagons are preferred over up-hexagons and the effect of C is stabilizing for $C<C_c$, while up-hexagons are preferred over down-hexagons and the effect of C is destabilizing for $C>C_c$. Figure 3 presents R_1 versus S_t at C=1.0 and for T=0.0, 0.25 and 0.50. It can be seen from our extensive generated data and from this figure that for T=0.0, R_1 is negative, $|R_1|$ is small, and the effect of S_t is destabilizing in the sense that subcritical effect is increased with increasing S_t. It turns out that for $T\neq 0$ and below T_{c2}, R_1 is negative for small S_t and $|R_1|$ decreases with increasing S_t until R_1 becomes zero at some critical S_{tc} of S_t. For

$S_t > S_{tc}$, R_1 is positive and increases with S_t. The value of S_{tc} is found to decrease with increasing T. For $T \neq 0$ and above T_{c2}, R_1, which is now positive, increases with S_t. The rate of increase of R_1 with respect of S_t in found to increase with T. Hence, in contrast to the non-rotating case, the tendency for the flow towards preference of down-hexagons increases with S_t in the range $S_t < S_{tc}$, while down-hexagons, which are actually preferred over up-hexagons in the range $S_t > S_{tc}$, become increasingly more significant as S_t increases beyond S_{tc}.

Referring to (30), it should be noted that R_{10}, which entirely due to the interactions between the local solid fraction and the Coriolis term in the momentum-Darcy equation, is zero for T=0.0 and negative for $T \neq 0$, and $|R_{10}|$ increases rapidly with T. However, R_{11}, which is due to these interactions as well as to other nonlinear interactions in the equations, can be either positive or negative depending on the parameter values. However, if the interactions between the local solid fraction and the Coriolis terms are not taken into account, then it was found that $R_{11} < 0$ for T below some critical value T_{c3} of T, where $R_1 < 0$ and $|R_1|$ decreases with increasing T until R_1 becomes zero at some value of T and then increases with further increases in T. Hence, preference of down-hexagons is mainly associated with positive value of R_{11} and these later interactions can be effective to make down-hexagons preferred over up-hexagons only for $T > T_{c3}$.

The coefficient R_{20}, given by (24c), for the hexagonal convection (N=3, $A_n = 1/\sqrt{6}$), designated here by $R_{20}^{(h)}$, was computed for various values of T, S_t, C, K_c and K_2. It was found that $R_{20}^{(h)}$ is always positive for both rotating and non-rotating cases. For T=0.0, it is independent of C, S_t and K_c, but it increases with K_2. For $T \neq 0$, $R_{20}^{(h)}$ is independent of S_t and K_c, increases with K_2 and T, and it decreases with increasing C. Some typical

results about the variation of $R_{20}^{(h)}$ with respect to C for T=0.12, 0.25 and 0.50 are presented in Figure 4 for K_2=0.0. It is seen from this figure that the rate of decrease of $R_{20}^{(h)}$ with respect to C is rather high for small C, and $R_{20}^{(h)}$ increases rapidly with T. If the interactions between the local solid fraction and the Coriolis term are not taken into account, then it was found that $R_{20}^{(h)}$ is still positive, independent of C, S_t and K_c, and it increases with K_2 and T . However, its value and its rate of increase with respect to T is rather small if such interactions are not taken into account. Although variations of R_1 with respect to different parameters provide information about various destabilizing and stabilizing features in the rotating case for the hexagonal convection, as was presented and discussed in the last two paragraphs, it should be noted that information about R_{20} for hexagons is useful in the sense that since R_{20} is the leading second-order coefficient in the expansion for R in powers of ε, $R_{20}^{(h)}$ plays useful roles in calculating the solute flux and the order of magnitude of ε in (31) and in cases where R_1 becomes negligible or for the stability consideration of hexagons that will be discussed further in the next sub-section.

We also examined the vertical distribution of solid fraction at different locations in the horizontal direction for the hexagonal convection. Our generated data at centers and at the nodes of hexagons indicated that the perturbation to solid fraction at the nodes is generally positive, while that at the centers is generally negative. This general result holds irrespective of the parameter values considered, which indicates tendency for the chimney formation at the cells' centers and not at the nodes contrary to the experimental result (Tait etal.1992). However, it should be noted that such experimental result were conducted at the Rayleigh number about one order of magnitude higher than that at the

onset of plume convection, while the present results are strictly valid close to the onset of plume convection. Unfortunately, no experimental results near the onset of plume convection, for either non-rotating or rotating case, are available yet to confirm the present theoretical result. In addition, our results indicate that rotational effect may be beneficial since the perturbation to solid fraction at any node in the rotating system is found to be higher in value at any vertical level than the corresponding one in the absence of rotation. Some typical results are presented in Figure 5 for the vertical distribution of the basic state and total solid fraction at center of a hexagon for T=0.0 and 0.5. In these calculations δ=0.2, S_t=C=1.0, K_c=K_2=0.0, and the value ε =0.002 is chosen, which is the maximum value of ε beyond which the solid fraction becomes negative. This is based on the physical ground that deviation of the total solid fraction $\tilde{\phi}$ from ϕ_B cannot be such that $\tilde{\phi}$ becomes negative. We have chosen zero values for K_c and K_2 in these calculations since $\tilde{\phi}$ is found to be much less sensitive with respect K_c and K_2 at such small value of ε. It is seen from this figure that the solid fraction in the rotating case is notably smaller than that in the absence of rotation, except close to the upper boundary, and, hence, tendency for the chimney formation at the cells' centers increases in the presence of rotation. Furthermore, the results also indicate that tendency for chimney formation is higher near the lower boundary than anywhere else in the layer.

Square pattern convection

We now present and discuss the result for another three-dimensional case of convection whose form is that of square cells, which, as is discussed later, could become prefer in the present problem for T in particular range of values. First referring back to the figure 5, which also provides graphs for the total solid fraction at a center of square

cell in the case of square pattern convection. The parameter conditions are as in the case of hexagons. Again the tendency for chimney formation increases in the presence of rotation and such tendency is stronger near the lower boundary. It is also seen from this figure that the tendency for chimney formation at the squares cells' centers is apparently higher than that at the hexagons cells' centers. Our additional generated data at the boundary points between two square cells indicated that the perturbation to solid fraction is negative and the tendency for chimney formation is higher in the presence of rotation.

As was explained in the previous section, R_1 is zero for the case where convection is in the form of square cells, and, thus, we next present and discuss the results for the coefficient R_{20}, given by (24c), for the square cells (N=2, A_n=1/2), which is designated here by $R_{20}^{(s)}$. This coefficient was computed for various values of T, S_t, C, K_c and K_2. It was found that, depending on the value of T, $R_{20}^{(s)}$ can be positive or negative and, thus, both supercitical and subcritical squares can be possible. Also, $R_{20}^{(s)}<R_{20}^{(h)}$ for both rotating and non-rotating cases. For T=0.0, $R_{20}^{(s)}$ is positive and independent of C, S_t and K_c, but it increases with K_2, which is consistent with the stabilizing effect of decreasing the permeability. For T≠0, $R_{20}^{(s)}$ is independent of S_t and K_c, increases with K_2 and T, and it decreases with increasing C. Thus, rotational constraint reverses the role of C in the nonlinear regime for squares. Some typical results about the variation of $R_{20}^{(s)}$ with respect to C for T=0.12, 0.25 and 0.50 are presented in Figure 6 for K_2=0.0. As in the case of $R_{20}^{(h)}$, it is seen from this figure that the rate of decrease of $R_{20}^{(s)}$ with respect to C is high for small C, and $R_{20}^{(s)}$ increases rapidly with T. The square pattern convection is supercritical in this range of values for T. If the interactions between the local solid fraction and the Coriolis term are not taken into account, then the qualitative features of

$R_{20}^{(s)}$ are similar to those of $R_{20}^{(h)}$ described before. We also determined some results about variation of $R_{20}^{(s)}$ with respect to T for different values of C. It was found from our calculated data that $R_{20}^{(s)}$ is positive for sufficiently small T and increases with T until $R_{20}^{(s)}$ reaches a maximum value at some critical $T=T_{c4}$. For $T>T_{c4}$, $R_{20}^{(s)}$ decreases with increasing T until $R_{20}^{(s)}$ becomes zero at some critical $T=T_{c5}$. For $T>T_{c5}$, squares are subcritical. The critical values for T_{c4} and T_{c5} are found to increase with C. In the subcritical regime, $R_{20}^{(s)}$ increases with C. These qualitative features of squares are found to be entirely due to the interactions between the local solid fraction and the Coriolis term.

Rectangular pattern convection

The simplest semi-regular solutions in the form of different types of rectangular patterns are found to become preferred in the present problem for T above some values T_{c6}. Similar to the case of squares, R_1 is zero for rectangles. For T just above the smallest value of T_{c6}, which is very slightly above zero, rectangles with angle γ about 60° are supercritical and their R_{20} value, which is designated for general rectangle by $R_{20}^{(re)}$, is smaller than the corresponding one for rolls. As is discussed later, there is an interesting pattern transitional phenomenon in the sense that γ increases continuously with T until γ reaches the value of 90° and the rectangles become squares. Each one of such rectangular cells solutions is found to have the smallest value of $R_{20}^{(re)}$ over some interval in T in the domain $60°<\gamma<90°$.

The qualitative results about the total solid fraction for the rectangles are found to be generally similar to those for squares presented and discussed before. The coefficient $R_{20}^{(re)}$, which is independent of K_c and S_t, was computed for various values of T, C, γ and

K_2. It was found that $R_{20}^{(re)}$ is positive for T below some critical value T_{c7} and negative for T above T_{c7}. Thus both supercritical and subcritical rectangles can exist in particular range of values for T. As in the case of squares, $R_{20}^{(re)}<R_{20}^{(h)}$. The qualitative results about variations of $R_{20}^{(re)}$ with respect to C and K_2 are similar to those for squares. Some typical results about the variations of R_{20} with respect to T and γ are shown in Figure 7 for C=1.0. It can be seen from this figure that the effect of increasing T is very slightly stabilizing for the supercritical rectangles at lower values of T and significantly destabilizing for higher values of T. The effect of increasingT is generally destabilizing for the subcritical rectangles. The effect of increasing γ is stabilizing for the rectangles.

Two-dimensional rolls

As was explained in the previous section, R_1 is zero for two-dimensional rolls. Thus, the important coefficient for rolls (N=1, $A_n=1/\sqrt{2}$) is R_{20} given in (24c), which is designated here by $R_{20}^{(r)}$. This coefficient was computed for various values of T, S_t, C, K_c and K_2. It was found that $R_{20}^{(r)}$ is always positive and, thus, such flow is supercritical. Also, $R_{20}^{(r)}<R_{20}^{(h)}$ for both rotating and non-rotating cases. However, as can be seen from the figure 7, $R_{20}^{(r)}$ is found to be smaller than $R_{20}^{(re)}$ for T below some critical value T_{c8}, and $R_{20}^{(r)}> R_{20}^{(re)}$ for $T>T_{c8}$. The value of T increases with C. For T=0.0, $R_{20}^{(r)}$ is independent of C, S_t and K_c, but it increases with K_2. For $T\neq0$, $R_{20}^{(r)}$ is independent of S_t and K_c, increases with K_2 and T, and it decreases with increasing C. Some calculated results about the variation of $R_{20}^{(r)}$ with respect to C for different values of T indicated that the rate of decrease of $R_{20}^{(r)}$ with respect to C is high for small C, and $R_{20}^{(r)}$ increases rapidly with T. If the interactions between the local solid fraction and the Coriolis term

are excluded from the present model, then the qualitative features of $R_{20}^{(r)}$ are similar to those of $R_{20}^{(h)}$ described before.

Figure 8 presents some typical results about comparison between the variation of the coefficient R_{20} with respect to T for rolls, squares and hexagons. The results are for C=1.0 and K_2 =0.0. It seen from this figure that rolls can be realized at a lower value of the Rayleigh number than squares for $T<T_{c8}$, while squares can be realized at a lower value of R for $T>T_{c8}$. In addition, supercritical hexagons are generally realized at a value of R larger than those due to rolls and squares.

Our calculated data for the vertical distribution of the solid fraction at locations between two rolls or at centers of the rolls indicated that the perturbation to the solid fraction at the centers of the rolls can be positive, while that at locations between two rolls is generally negative. Hence, tendency for the chimney formation is more at locations between the rolls. In addition, it was found that the tendency for chimney formation increases slightly in the presence of rotation, and such tendency is significantly higher in a region near the lower boundary.

4.2. Stability of finite-amplitude steady solutions

Following standard stability procedure (Schluter et al.1965;Busse1967), the system (28b) for the growth rate σ^* of the disturbances acting on the finite-amplitude steady solutions has been simplified, and the expression for σ^* has been computed for different integers N and various values of the quantities Φ_{nm} ($|\Phi_{nm}|\leq 1$) and Ψ_{nm} ($|\Psi_{nm}|\leq 1$). In all the cases that have been investigated only steady supercritical solutions in the form of rolls, rectangles and squares, and subcritical steady solutions in the form of down-hexagons and up-hexagons are found to be possibly stable in particular range of values

for the non-dimensional parameters and for ε. The results are briefly as follows.

Supercritical rolls are stable only if

$$|\varepsilon| \geq \varepsilon_1,\ \varepsilon_1 = \sqrt{3}|R_1|/R_{20}^{(r)},\ 0 < R_{20}^{(r)} \leq R_{20}^{(s)},\ 0 < R_{20}^{(r)} \leq R_{20}^{(re)}. \tag{33a}$$

Supercritical squares are stable only if

$$|\varepsilon| \geq \varepsilon_2,\ \varepsilon_2 = \sqrt{3}|R_1|/[\sqrt{2}(R_{20}^{(r)} - R_{20}^{(s)})],\ R_{20}^{(r)} > R_{20}^{(s)} > 0,\ R_{20}^{(re)} \geq R_{20}^{(s)} > 0. \tag{33b}$$

Supercritical rectangles are stable only if

$$|\varepsilon| \geq \varepsilon_3,\ \varepsilon_3 = \sqrt{3}|R_1|/[\sqrt{2}(R_{20}^{(r)} - R_{20}^{(re)})],\ R_{20}^{(r)} > R_{20}^{(re)} > 0,\ R_{20}^{(s)} \geq R_{20}^{(re)} > 0. \tag{33c}$$

Subcritical down-hexagons are stable only if

$$\varepsilon_4 \leq |\varepsilon| \leq \varepsilon_5,\ \varepsilon_4 = |R_1|/R_{20}^{(h)},\ \varepsilon_5 = 6|R_1|/(R_{20}^{(h)} - R_{20}^{(r)}),\ R_1 > 0. \tag{33c}$$

Subcritical up-hexagons are stable only if

$$\varepsilon_4 \leq |\varepsilon| \leq \varepsilon_5,\ R_1 < 0. \tag{33d}$$

Figure 9 provides a qualitative bifurcation diagram representing the amplitude ε versus R for those solutions, which can possibly be stable in particular range of ε according to the results provided in (33). Solid lines correspond to linearly stable branches while dotted lines correspond to linearly unstable branches. Note that no representation is given in this diagram of a three-dimensional solution that is always unstable. This bifurcation diagram provides different cases for possibly stable solutions. For $T < T_{c8}$, two-dimensional roll-branch bifurcates supercritically and is initially unstable to a subcritically bifurcating hexagonal branch. The hexagonal branch either is due to up-hexagons if ε is positively upward in the diagram or is due to down-hexagons if ε is positively downward in the diagram. For $T_{c8} < T < T_{c5}$, square-branch bifurcates supercritically and is initially unstable to a subcritically bifurcating hexagonal branch.

For $T_{c6}<T<T_{c7}$, rectangular branch bifurcates supercritically and is initially unstable to subcritically bifurcating hexagonal branch.

5. Conclusion and some remarks

We investigated the problem of nonlinear steady convection in a rotating mushy layer during alloy solidification. We analyzed the two- and three-dimensional steady modes of convection in the rotating mushy layer using the model due to Amberg and Homsy (1993). We performed a weakly nonlinear analysis by taking into account all the linear and nonlinear interaction terms, including those between the local solid fraction and the flow associated with the Coriolis term, in the governing equations to determine the steady solutions admitted by the nonlinear problem and employed stability analysis to determine the solutions that can be stable with respect to arbitrary three-dimensional disturbances in different ranges of the parameter values and the amplitude of motion ε. We found that, depending on the range of values of the parameters and ε, two-dimensional oblique rolls and distorted three-dimensional solutions in the form of squares, rectangles, down-hexagons and up-hexagons can be possibly stable. We found that two-dimensional rolls are supercritical and stable only if ε is equal to or above some value ε_1 and T is below some values T_{c6} and T_{c8} or above some values T_{c5} and T_{c7}. Three-dimensional squares (rectangles) are stable only if they are supercritical, ε is equal to or above some value ε_2 (ε_3) and T lies in the range $T_{c8}<T<T_{c5}$ ($T_{c6}<T<T_{c7}$). Subcritical squares and subcritical rectangles also can exist but they are unstable. Subcritical down-hexagons are stable only if ε lies in the range $\varepsilon_4 \le \varepsilon \le \varepsilon_5$ and $R_1>0$. Subcritical up-hexagons are stable only if ε lies in the range $\varepsilon_4 \le \varepsilon \le \varepsilon_5$ and $R_1<0$. Supercritical down-hexagons and supercritical up-hexagons

also can exist but they are unstable. There are certain overlap regions in ε where more than one solution can be stable and, thus, hysteretic effect can be non-zero in such overlap regions. Our results of the studies of the onset of plume convection and chimney formation within the mushy layer indicated that the chimney of the plume could be initiated most likely near the lower boundary of the layer. Presence of rotation was found to reduce the tendency for chimney formation at centers of rolls and at the nodes on the boundary of hexagons. The stability of supercritical rectangles and squares uncovered in the present study was found to be entirely due to the interactions between the local solid fraction and the Coriolis term in the momentum-Darcy equation, and such interactions were also found to enhance significantly the stability of the subcritical down-hexagons.

As we referred to earlier in the section1, Guba (2001) studied the problem of finite-amplitude steady convection in a rotating mushy layer under the condition where the interactions between the local solid fraction and the Coriolis term were not taken into account. The author carried out a weakly nonlinear analysis of two-dimensional oblique rolls and distorted hexagons, by calculating only the leading non-zero coefficient beyond R_c in the expansion for R for each of such solutions, but no stability analysis was made of these finite-amplitude solutions. Similar to the work due to Amberg and Homsy (1993), Guba (2001) studied the case where the permeability coefficient K_1 can be in general an order one quantity and predicted, similar to that due to Amberg and Homsy (2001), that depending on the range of the parameter values, either subcritical or supercritical rolls can exist, and the subcritical hexagons can change the form from up-hexagons to down-hexagons for T beyond some critical value. It should, however, be noted that one can show that such subcritical rolls as well as the hexagonal solutions found by Guba are

unstable. Also, as was shown in the present study, the supercritical rolls found by Guba cannot be realizable over certain range of values of T, provided the interaction terms between the local solid fraction and the Coriolis term are taken into account. Guba's results were reported for T as large as 7. However, as was found in the present study, if the interaction terms between the local solid fraction and the Coriolis term as taken into account in the study to determine the results, then the validity of the results for T>1 is mostly questionable since $|R_1|$ and $|R_{20}|$ can become much larger than unity by about 2 to 3 orders of magnitude for T just above unity, so that the modeling assumption of the type (8), which assumes that the coefficients, such as $|R|$ and $|R|$, in those double-expansions in powers of ε and δ be of order unity, can no longer be justified.

In the present study and as presented in the first paragraph in this section, we were interested to carry out a significant extension of the work by Guba (2001) by fully including the interaction terms between the local solid fraction and the Coriolis term, carrying out weakly nonlinear analysis to determine all the two- and three-dimensional steady solutions admitted by the nonlinear system and performing the stability analyses of the finite-amplitude solutions to determine all the possible stable solutions. During our extensive investigation, we were able to uncover significant new results and new flow features that can increase our understanding of the effects of an external constraint of rotation on the flow in the mushy layers and hopefully could aid future researchers for further studies in the area. In regard to comparison of the present results to some experimental results, it should be noted that all the available experimental results, which are due to Sample and Hellawell (1982, 1984) and Claben et al. (1999), have been for cases of fully nonlinear convection with fully developed chimneys, and, thus, they cannot

be applicable for comparison with the present results for the weakly nonlinear convection near the onset of motion. It is hoped that some experimental studies of the present problem could be carried out by some experimentalists in near future for a comparison with the present qualitative results. As was shown by Guba (2001), the case $T \leq 1$ can be quite accessible in the laboratory for ammonium chloride-water system since it yields a value of the rotation rate about $\omega \leq 2.0$ rad/s.

Appendix A

The expressions for the coefficients $V_{01}^*(z)$, $\psi_{01}^*(z)$, $\theta_{01}^*(z)$ and $\phi_{01}^*(z)$ are given below

$$(V_{01}^*, \theta_{01}^*)=(b_1, c_1)\, z \sin(\pi z)+(b_2, c_2) z \cos(\pi z)+(b_3, c_3) z^2 \cos(\pi z)+(b_4, c_4)\sinh(rz)+(b_5, c_5)\cosh(rz)+(b_6, c_6)\cos(\pi z)+(b_7, c_7)\sin(\pi z), \quad \text{(A1a)}$$

$$\psi_{01}^*=T\{b_1[\sin(\pi z)+\pi z\cos(\pi z)]+b_2[\cos(\pi z)-\pi z\sin(\pi z)]+b_3[2z\cos(\pi z)-\pi z^2\sin(\pi z)]+b_4 r\cosh(rz)+b_5 r\sinh(rz)-b_6\pi\sin(\pi z)+\pi[b_7+(1-z)(\pi^2+a^2)/(CR_{00}a^2)]\cos(\pi z)\}, \quad \text{(A1b)}$$

$$\phi_{01}^*=b_0+(R_{00}a^2/C)\{b_1[-(z/\pi)\cos(\pi z)+(1/\pi^2)\sin(\pi z)]+b_2[(z/\pi)\sin(\pi z)+(1/\pi^2)\cos(\pi z)]+b_3[(z^2/\pi)\sin(\pi z)+(2/\pi^2)z\cos(\pi z)-(2/\pi^3)\sin(\pi z)]+(b_4/r)\cosh(rz)+(b_5/r)\sinh(rz)+(b_6/\pi)\sin(\pi z)-(b_7/\pi)\cos(\pi z)\}-[(2R_{01}+R_{00})a^2(\pi^2+a^2)/(2C\pi R_{00}a^2)+1/(\pi C^2)](\pi^2+a^2)\cos(\pi z)+(1/C)[1-(\pi^2+a^2)/(C\pi^2)]\sin(\pi z)+(-1+1/C)(\pi^2+a^2)[1/(\pi C)][-z\cos(\pi z)+(1/\pi)\sin(\pi z)]-[(\pi^2+a^2)/(\pi C^2)]z, \quad \text{(A1c)}$$

where

$$b_2=(\pi^2+a^2)[2R_{01}+R_{00}/2-2\pi^2T^2(\pi^2+a^2)/(Ca^2R_{00})]/d_1,\ d_1\equiv 2\pi[2\pi^2(1+T^2)+a^2(2+T^2)], \quad \text{(A1d)}$$

$$r=\{[a^2(2+T^2)+d_0^{0.5}]/(2+2T^2)\}^{0.5},\ d_0\equiv a^2[a^2(2+T^2)^2-4(a^2-R_{00}^2)(1+T^2)], \quad \text{(A1e)}$$

$$b_3=(\pi^2+a^2)[-R_{00}+2\pi^2T^2(\pi^2+a^2)/(Ca^2R_{00})]/(2d_1), \quad \text{(A1f)}$$

$$b_1=\{-R_{00}+2\pi T^2(\pi^2+a^2)(a^2+3\pi^2)/(a^2R_{00}C)-b_3[2a^2(2+T^2)+12\pi^2(1+T^2)]\}/d_1, \quad \text{(A1g)}$$

$b_4=(\pi^2 d_2+d_3)/[(\pi^2+r^2)\sinh(r)]$, $d_2\equiv b_3+[1+\cosh(r)](2\pi b_1+2b_3-d_4)/(\pi^2+r^2)$, $d_4\equiv 2\pi T^2(\pi^2+a^2)/[R_{00}a^2C(1+T^2)]$, $d_3\equiv -d_4+2\pi b_1+(2-\pi^2)b_3+[\pi^2-r^2\cosh(r)](d_4-2\pi b_1-2b_3)/(\pi^2+r^2)$, (A1h)

$$b_5=(d_4-2\pi b_1-2b_3)/(\pi^2+r^2)= -b_6,\ b_7=1, \tag{A1i}$$

$$c_1=[-\pi(1+T^2)(\pi b_1+4b_3)-a^2b_1+2\pi^2T^2(\pi^2+a^2)/(a^2CR_{00})]/R_{00}, \tag{A1j}$$

$$(c_2, c_3)=(b_2, b_3)[-\pi^2(1+T^2)-a^2]/R_{00}, \tag{A1k}$$

$$(c_4, c_5)=(b_4, b_5)[r^2(1+T^2)-a^2]/R_{00}, \tag{A1l}$$

$$c_6=[(1+T^2)(-\pi^2 b_6+2\pi b_1+2b_3)-a^2b_6-2\pi T^2(\pi^2+a^2)/(a^2CR_{00})]/R_{00}, \tag{A1m}$$

$$c_7=[(1+T^2)(-\pi^2-2\pi b_2)-a^2+R_{01}-2\pi^2T^2(\pi^2+a^2)/(a^2CR_{00})]/R_{00}. \tag{A1n}$$

The expressions for $V_{10}^*(z)$, $\psi_{10}^*(z)$, $\theta_{10}^*(z)$, $\phi_{10}^*(z)$, $V_{10}\hat{}(z, \Phi_{lp})$, $\psi_{10}\hat{}(z, \Phi_{lp})$, $\theta_{10}\hat{}(z, \Phi_{lp})$ and $\phi_{10}\hat{}(z, \Phi_{lp})$ are given below

$(V_{10}^*, \theta_{10}^*)=(b_8, c_8)z\cos(\pi z)+(b_9, c_9)\sinh(rz)$, $(b_8, c_8)\equiv R_{10}\{1/[2\pi(1+T^2)], -(\pi^2+a^2)/(2\pi R_{00})\}$, $b_9\equiv b_8/\sinh(r)$, $c_9\equiv -b_9R_{00}a^2/(r^2+a^2)$, (A2a)

$$\psi_{10}^* =T[rb_9\cosh(rz)+b_8\cos(\pi z)-\pi b_8 z\sin(\pi z)], \tag{A2b}$$

$\phi_{10}^*=(R_{00}a^2/C)\{(b_8/\pi^2)[1+\pi z\sin(\pi z)+\cos(\pi z)]+b_9[\cosh(rz)-\cosh(r)]/r\}-R_{10}(\pi^2+a^2)[1+\cos(\pi z)]/(\pi CR_{00})$, (A2c)

$V_{10}\hat{}=b_{10}\sin(\pi z)+b_{11}\sin(2\pi z)$, $b_{10}\equiv(a_{lp}^2+\pi^2)(2\pi T^2/C)(\pi^2+a^2)^2/\{2a^2R_{00}[(a_{lp}^2+\pi^2)(a_{lp}^2+\pi^2+\pi^2T^2)-a_{lp}^2R_{00}^2]\}$, $a_{lp}^2\equiv 2a^2(1+\Phi_{lp})$, $b_{11}\equiv[\pi(T^2/C)(\pi^2+a^2)^2(a_{lp}^2+4\pi^2)/(a^2R_{00})-\pi R_{00}(\pi^2+a^2)(1-\Phi_{lp})/2]/\{(a_{lp}^2+4\pi^2)[a_{lp}^2+4\pi^2(1+T^2)]-R_{00}^2a_{lp}^2\}$, (A2d)

$\theta_{10}\hat{}=c_{10}\sin(\pi z)+c_{11}\sin(2\pi z)$, $c_{10}\equiv -R_{00}a_{lp}^2b_{10}/(a_{lp}^2+\pi^2)$, $c_{11}\equiv[\pi(\pi^2+a^2)(1-\Phi_{lp})/2-R_{00}a_{lp}^2b_{11}]/(a_{lp}^2+4\pi^2)$, (A2e)

$$\psi_{10}\hat{}=T\{-(\pi^2+a^2)^2\cos(\pi z)[1+\cos(\pi z)]/(2CR_{00}a^2)+\pi b_{10}\cos(\pi z)+2\pi b_{11}\cos(2\pi z)\}, \tag{A2f}$$

$\phi_{10}\hat{}=[R_{00}a_{lp}^2/(\pi C)]\{-[1+\cos(\pi z)]b_{10}+[1-\cos(2\pi z)]b_{11}/2\}+(\pi^2+a^2)(1-\Phi_{lp})[\cos(2\pi z)-$

1]/(4C). (A2g)

The expressions for the coefficients F_{11} and G_{11} are given below

$F_{11}=[-R_{00}/(\pi^2+a^2)]\{K_c(\pi^2+a^2)^3[\pi^2(1-T^2)(1+\Phi_{lp})+a_{lp}^2]/(2\pi CR_{00}^2a^2)+ K_2(\pi^2+a^2)^3[(\pi^2+a_{lp}^2)(9\pi^2+16)/(18\pi^2)+20/9+(28/9+ \pi^2/2)\Phi_{lp}-\pi^2T^2(1+\Phi_{lp})(9\pi^2+56)/(18\pi^2)]+\pi T^2(\pi^2+a^2)^3(1+\Phi_{lp})[1+56/(9\pi^2)-2\pi C^2E_5/(\pi^2+a^2)]+T(\pi^2+a^2)^2[(E_4+ \pi TE_1+\pi TE_2)(1+\Phi_{lp})+ \pi E_6/(\pi^2a^2+a^4)]/(CR_{00})-\pi(\pi^2+a^2)(1+\Phi_{lp}/2)E_3-R_{00}\pi a^2E_2(1/2+\Phi_{lp})+2c_{11}/(3\pi)-R_{01}(\pi^2+a^2)c_{10}a_{lp}^2/(2a^2R_{00})+(S_tR_{00}/C+R_{01})b_{10}a_{lp}^2/2+8R_{00}a_{lp}^2b_{11}/(9\pi^2)-T^2(\pi^2+a^2)\pi a_{lp}^2[\pi b_{10}/4+20b_{11}/(9\pi)]/(CR_{00}a^2)\}$, (A3a)

$G_{11}=[-R_{00}/(\pi^2+a^2)]\{\pi TE_7(\pi^2+a^2)/(CR_{00}a^2)-R_{01}(\pi^2+a^2)[c_9E_8-c_8/(4\pi)]-R_{10}(\pi^2+a^2)E_9/R_{00}-T^2(\pi^2+a^2)\pi [b_8/4+rb_9(E_{10}-E_{11})]/(CR_{00})+\pi c_8/4-rc_9E_{12} -S_tR_{00}a^2b_9E_8/r +S_tR_{10}(\pi^2+a^2)a^2/(2C^2) + R_{00}a^2[b_8/(4\pi)+b_9(E_8-2E_{13})]/2+R_{01}a^2[-b_8/(4\pi)+b_9E_8]+R_{10}a^2E_1\}$, (A3b)

where

$E_1=\langle V_{01}^*\sin(\pi z)\rangle$, $E_2=\langle V_{01}^*\sin(2\pi z)\rangle$, $E_3=\langle\theta_{01}^*\sin(2\pi z)\rangle$,

$E_4=\langle\psi_{01}^*\cos(\pi z)[1+\cos(\pi z)]\rangle$, $E_5=\langle\phi_{01}^*\cos^2(\pi z)\rangle$, $E_6=a_{lp}^2\langle(z-1)\psi_{10}\hat{}\cos(\pi z)\rangle$, $E_7=a^2\langle(z-1)\psi_{10}^*\cos(\pi z)\rangle$, $E_8=\langle\sin(\pi z)\sinh(rz)\rangle$, $E_9=\langle\theta_{01}^*\sin(\pi z)\rangle$, $E_{10}=\langle\sin(\pi z)\cosh(rz)\rangle$, $E_{11}=\langle z\cos(\pi z)\cosh(rz)\rangle$, $E_{12}=\langle\sin(\pi z)\cosh(rz)\rangle$, $E_{13}=\langle z\sin(\pi z)\sinh(rz)\rangle$. (A3c)

The expressions for F_{20}, H_{20} and G_{20} are given below

$F_{20}=[-R_{00}/(\pi^2+a^2)]\{K_2(\pi^2+a^2)^4[-5\pi^2-10a^2(3/2+\Phi_{ml}+\Phi_{mp}+\Phi_{lp})-2\pi^2(1+7\Phi_{lp})+7T^2R_{00}\pi^2(\Phi_{ml}+\Phi_{mp})+7T^2\pi^2]/(8C^2R_{00}^2a^2\pi^2)-T^2(\pi^2+a^2)\pi^2[2(1+\Phi_{ml}+\Phi_{mp})E_{14}+7(\pi^2+a^2)^2(1+\Phi_{ml}+\Phi_{mp})/(8\pi^2C^2)+a^2R_{00}(2+2\Phi_{lp}+\Phi_{ml}+\Phi_{mp})E_{15}/(T\pi^2Ca_{lp}^2) -R_{00}(a_{lp}^2+\Phi_{ml}+\Phi_{mp})E_{16}/(\pi^2C)+7(\pi^2+a^2)^2(1+\Phi_{ml}+\Phi_{mp})/(\pi^2C^2)]- \pi(\pi^2+a^2)E_{17}(2+\Phi_{ml}+\Phi_{mp})/2-\pi R_{00}a^2E_{18}(1+\Phi_{lp}+\Phi_{ml}+\Phi_{mp})\}$, (A4a)

$H_{20}=[-R_{00}/(\pi^2+a^2)]\{R_{10}a_{lp}^2[b_{10}-(\pi^2+a^2)c_{10}/(a^2R_{00})]/2- T(\pi^2+a^2)^2(1+\Phi_{lp})[E_{19}+2T\pi^2CE_{20}/R_{00}-Ta^2\pi(E_{21}+E_{22})]-\pi(\pi^2+a^2)(1+\Phi_{lp}/2)E_{23}-\pi R_{00}a^2E_{22}(1/2+\Phi_{lp})\}$, (A4b)

$G_{20}=[-R_{00}R_{10}a^2/(\pi^2+a^2)][-b_8/(4\pi)+\pi b_9\sinh(r)/(\pi^2+r^2)]+R_{10}[-c_8/(4\pi)$

$+\pi\sinh(r)/(\pi^2+r^2)]$, (A4c)

where

$E_{14}=<\phi_{10}\hat{}\cos^2(\pi z)>$, $E_{15}=-a_{lp}{}^2<\psi_{10}\hat{}\cos(\pi z)[1+\cos(\pi z)]>$, $E_{16}=<(dV_{10}\hat{}/dz)\cos(\pi z)$

$[1+\cos(\pi z)]>$, $E_{17}=<\theta_{10}\hat{}\sin(2\pi z)>$, $E_{18}=<V_{10}\hat{}\sin(2\pi z)>$, $E_{19}=-a^2<\psi_{10}{}^*\cos(\pi z)[1+$

$\cos(\pi z)]>$, $E_{20}=<\phi_{10}{}^*\cos^2(\pi z)>$, $E_{21}=<V_{10}{}^*\sin(\pi z)>$, $E_{22}=<V_{10}{}^*\sin(2\pi z)>$, $E_{23}=<\theta_{10}{}^*\sin(2\pi$

$z)>$. (A4d)

Appendix B

The stability system for the present problem is given below

$\nabla^2\{\varepsilon[K_1\phi'+K_2(2\phi_B+2\varepsilon\phi)\phi']\Delta_2V+K(\phi_B+\varepsilon\phi)\Delta_2V'\}+(\partial/\partial z)\{\varepsilon\Omega V.\nabla[K_1\phi'+K_2(2\phi_B$

$+2\varepsilon\phi)\phi']+\Omega V'\cdot\nabla K(\phi_B+\varepsilon\phi)\}+(\partial/\partial z)\{\varepsilon[(\partial/\partial x)(K_1\phi'+2K_2\phi_B\phi'+2K_2\varepsilon\phi\phi')(\partial\psi/\partial y)-(\partial/\partial y)(K_1$

$\phi'+2K_2\phi_B\phi'+2K_2\varepsilon\phi\phi')(\partial\psi/\partial x)]+[(\partial/\partial x)K(\phi_B+\varepsilon\phi)(\partial\psi'/\partial y)-(\partial/\partial y)K(\phi_B+\varepsilon\phi)(\partial\psi'/\partial x)]\}-$

$R\Delta_2\theta'+T(\partial/\partial z)\{(\partial/\partial y)[(\partial\psi'/\partial y+\partial^2V'/\partial x\partial z)/(1-\phi_B-\varepsilon\phi)+\varepsilon(\partial\psi/\partial y+\partial^2$

$V/\partial x\partial z)(1+2(\phi_B+\varepsilon\phi)+3(\phi_B+\varepsilon\phi)^2)\phi'+(\partial/\partial x)[(\partial\psi/\partial x-\partial^2V/\partial y\partial z)(1+2(\phi_B+\varepsilon\phi)+3(\phi_B+\varepsilon\phi)^2$

$)\phi']\}=0$, (B1a)

$\varepsilon[K_1\phi'+2K_2(\phi_B+\varepsilon\phi)\phi']\Delta_2\psi+K(\phi_B+\varepsilon\phi)\Delta_2\psi'+\varepsilon(\partial^2V/\partial x\partial z+\partial\psi/\partial y)(\partial/\partial y)[K_1\phi'+2K_2$

$(\phi_B+\varepsilon\phi)\phi']+(\partial^2V'/\partial x\partial z+\partial\psi'/\partial y)(\partial/\partial y)K(\phi_B+\varepsilon\phi)-(\partial^2V'/\partial y\partial z-\partial\psi'/\partial x)(\partial/\partial x)K(\phi_B+\varepsilon\phi)-$

$\varepsilon(\partial^2V/\partial y\partial z-\partial\psi/\partial x)(\partial/\partial x)[K_1\phi'+2K_2(\phi_B+\varepsilon\phi)\phi']-T\{(\partial/\partial x)[(\partial\psi'/\partial y+\partial^2V'/\partial x\partial z)/(1-$

$\phi_B-\varepsilon\phi)+\varepsilon(\partial\psi/\partial y+\partial^2V/\partial x\partial z)(1+2(\phi_B+\varepsilon\phi)+3(\phi_B+\varepsilon\phi)^2)\phi']+(\partial/\partial y)[(-\partial\psi'/\partial x+\partial^2V'/\partial y\partial z)/(1-$

$\phi_B-\varepsilon\phi)+\varepsilon(-\partial\psi/\partial x+\partial^2V/\partial y\partial z)(1+2(\phi_B+\varepsilon\phi)+3(\phi_B+\varepsilon\phi)^2)\phi']\}=0$, (B1b)

$(\partial/\partial t-\delta\partial/\partial z)(-\theta'+S_t\phi')+R(d\theta_B/dz)\Delta_2V'+\nabla^2\theta'=\varepsilon R[(\Omega V+E\psi).\nabla\theta'+(\Omega V'+E\psi').\nabla\theta]$, (B1c)

$(\partial/\partial t-\delta\partial/\partial z)[(-1+\phi_B)\theta'+\theta_B\phi'+\varepsilon\phi\theta'+\varepsilon\phi'\theta-C\phi'/\delta]+R(d\theta_B/dz)\Delta_2 V' =R\varepsilon[(\Omega V+E\psi).\nabla\theta'$

$+(\Omega V'+E\psi').\nabla\theta]$, (B1d)

$$V'=\theta'=0 \text{ at } z=0, \quad \text{(B1e)}$$

$$V'=\theta'=\phi' \text{ at } z=1. \quad \text{(B1f)}$$

The expressions for L_{10}, L_{11}, L_{20} and $\tilde{F}_{20}$ are given below

$$L_{10}= -\pi[(\pi^2+a^2)^2/(CR_{00}a^2)][T^2(1+\Phi_{lp})+(T/2)(1+T^2)\Psi_{lp}], \quad \text{(B2a)}$$

$L_{11}=[F_{11}(\Phi_{lp})+H_{11}\Psi_{lp}]$, $H_{11}=\{K_c\pi(\pi^2+a^2)^2T/(2CR_{00}a^2)+ TK_2\pi(\pi^2+a^2)^2[1+C/2+56/(9\pi^2)]$

$/(C^2R_{00}a^2)-\pi T(\pi^2+a^2)^2[1/2+28/(9\pi^2)]/(C^2R_{00}a^2)-T(\pi^2+a^2)E_{16}/C-T^3\pi^2(\pi^2+a^2)E_5/(R_{00}a^2)+$

$T^3\pi(\pi^2+a^2)^2[1/2+28/(9\pi^2)]/(C^2R_{00}a^2)+T^2(\pi^2+a^2)E_4/C+[R_{00}^2a^2E_{24}/(\pi^2+a^2)-\pi TE_3R_{00}/2$

$+\pi TE_5\}$, (B2b)

$L_{20}=[H_{20}(\Phi_{lp})+\tilde{H}_{20}\Psi_{lp}]$, $\tilde{H}_{20}=\{T(\pi^2+a^2)\pi^2E_{20}/(R_{00}a^2)+T(\pi^2+a^2)\pi(E_{21}+E_{22})/C+\pi R_{00}TE_{23}/2-$

$R_{00}^2E_{25}/(\pi^2+a^2)+T^2(\pi^2+a^2)E_{19}/(Ca^2)-\pi^2T^3(\pi^2+a^2)E_{20}/(R_{00}a^2)\}$, (B2c)

$\tilde{F}_{20}=\{-7T(\pi^2+a^2)^3(K_2+CT^2R_{00}/2)/(4C^2R_{00}^2a^2)+T\pi^2(\pi^2+a^2)(1-T^2E_{14})/(R_{00}a^2)+T(\pi^2+a^2)(E_{16}$

$+TE_{15}/a_{lp}^2)/C+\pi TR_{00}E_{17}/2-R_{00}^2a^2E_{26}/[(\pi^2+a^2)a_{lp}^2]\}$, (B2d)

Where

$E_{24}=\langle\psi_{01}^*\sin^2(\pi z)\rangle$, $E_{25}=-a^2\langle\psi_{10}^*\sin^2(\pi z)\rangle$, $E_{26}=-a_{lp}^2\langle\psi_{10}\hat{}\sin^2(\pi z)\rangle$. (B2e)

REFERENCES

AMBERG, G. AND HOMSY, G. M. 1993 Nonlinear analysis of buoyant convection in binary solidification with application to channel formation. J. Fluid Mech. **252**, 79-98.

ANDERSON, D. M. AND WORSTER, M. G. 1995 Weakly nonlinear analysis of convection in mushy layers during the solidification of binary alloys. J. Fluid Mech. **302**, 307-331.

BUSSE, F. H. 1967 The stability of finite-amplitude convection and its relation to an extremum principal. J. Fluid Mech. **30**, 625-649.

BUSSE, F. H. 1989 Fundamentals of thermal convection. In Mantle Convection, Plate Tectonics and Global Dynamics, edited by W. R. Peltier, Gordon and Breach Science Publishers, New York, 23-95.

BUSSE, F. H. AND RIAHI, D. N. 1980 Nonlinear convection in a layer with nearly insulating boundaries. J. Fluid Mech. **96**, 243-256.

CHANDRASEKHAR, S. 1961 Hydrodynamic and Hydromagnetic Stability, Oxford: Clarendon Press.

CLABEN, S., HEIMPEL, M. AND CHRISTENSEN, U. 1999 Blob instability in rotating compositional convection. Geophys. Res. Lett. **26**, 135-138.

FOWLER, A. C. 1985 The formation of freckles in binary alloys. IMA J. Appl. Maths **35**, 159-174.

GORKOV, L. P. 1957 Stationary convection in a plane liquid near the critical leat transfer point. Sov. Phys. J. E. T. P. **6**, 311-315.

GUBA, P. 2001 On the finite-amplitude steady convection in rotating mushy layers. J. Fluid Mech. **437**, 337-365.

NEILSON, D. G. AND INCROPERA, F. P. 1993 Effect of rotation on fluid motion and channel formation during unidirectional solidification of a binary alloy. Int. J. Heat Mass Transfer **36**, 489-505.

NIELD, D. A. 1998 Instability and turbulence in convective flows in porous media. In Nonlinear Instability, Chaos and Turbulence, edited by L. Debnath and D. N. Riahi, WIT Press, UK, **1**, 225-276.

RIAHI, D. N. 1993 Effect of rotation on the stability of the melt during the solidification of a binary alloy. Acta Mechanica **99**, 95-101.

SAMPLE, A. K. AND HELLAWELL, A. 1982 The effect of mold precession on channel and macro-segregation in ammonium chloride-water analog casting. Metall. Trans. B **13**, 495-501.

SAMPLE, A. K. AND HELLAWELL, A. 1984 The mechanisms of formation and prevention of channel segregation during alloy solidification. Metall. Trans. A. **15**, 2163-2173.

SCHLUTER, A., LORTZ, D. AND BUSSE, F. H. 1965 On the stability of finite amplitude convection. J. Fluid Mech. **23**, 129-144.

TAIT, S., JAHRLING, K. AND JAUPART, C. 1992 The planform of compositional convection and chimney formation in a mushy layer. Nature **359**, 406-408.

WORSTER, M. G. 1992 Instabilities of the liquid and mushy regions during solidification of alloys. J. Fluid Mech. **237**, 649-669.

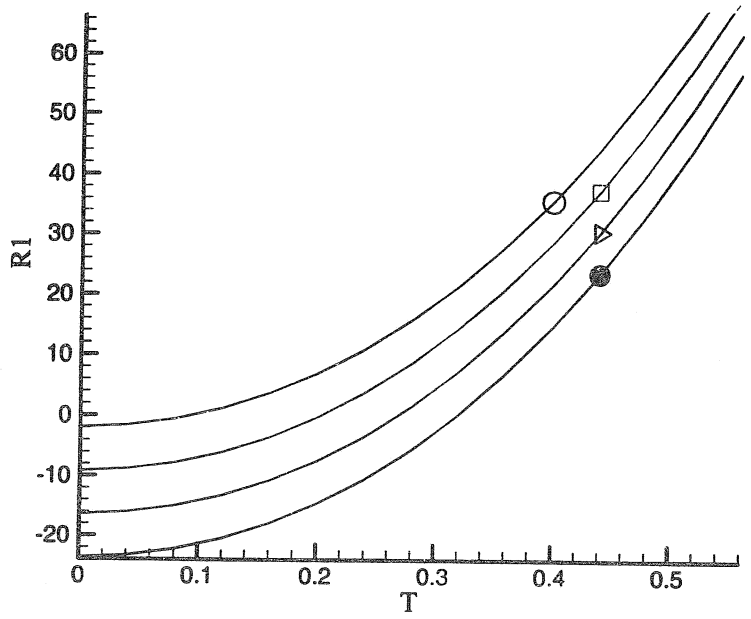

Figure 1. R_1 against T for hexagons. Here S_t=5.0, C=1.0 and K_2=0.0. The graphs labeled by the symbols of circle, square, triangle and filled circle present, respectively, R_1 for K_c=0.0, 1.0, 2.0 and 3.0.

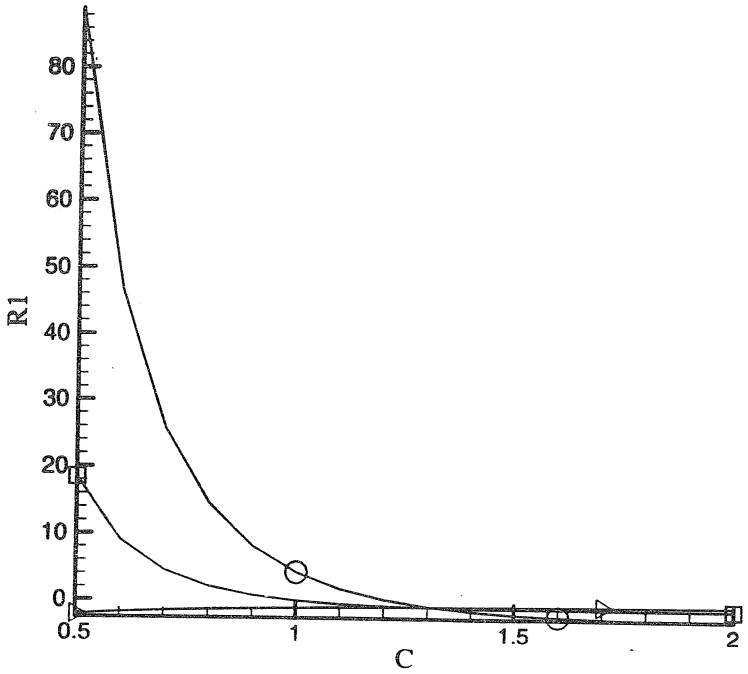

Figure 2. R_1 against C for hexagons. Here S_t=1.0, K_c=0.1 and K_2=0.0. The graphs labeled by the symbols of triangle, square and circle present, respectively, R_1 for T=0.0, 0.25 and 0.50.

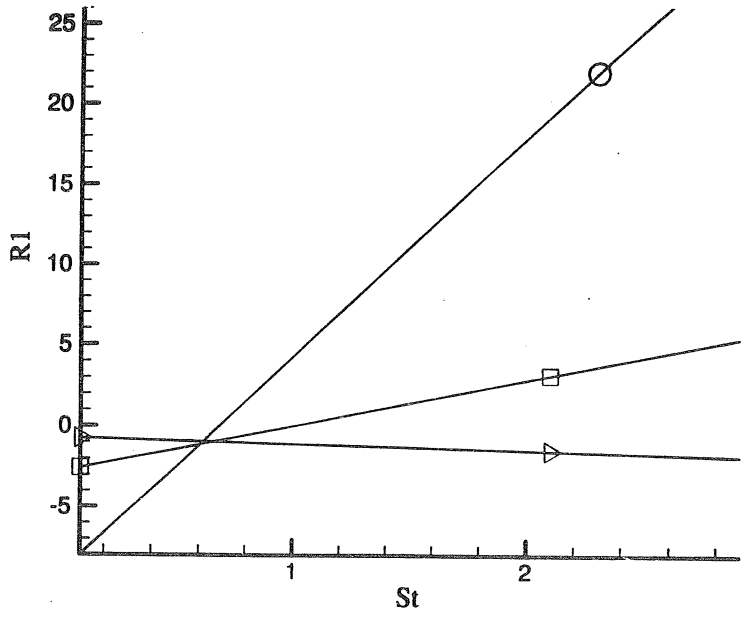

Figure 3. R_1 against S for hexagons. Here C=1.0, K_c=0.1 and K_2=0.0. The graphs labeled by the symbols of triangle, square and circle present, respectively, R_1 for T=0.0, 0.25 and 0.50.

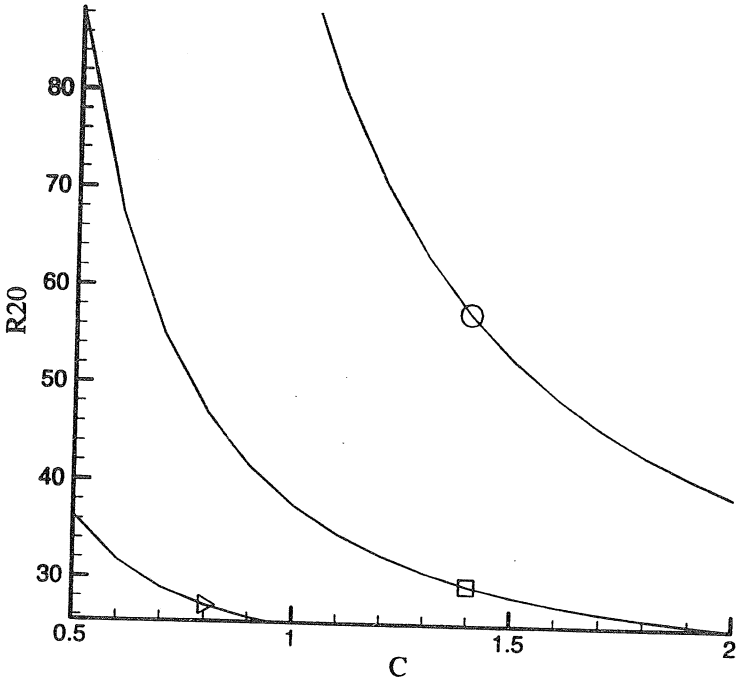

Figure 4. R_{20} against C for hexagons. Here S_t=1.0 and K_2=0.0. The graphs labeled by the symbols of triangle, square and circle present, respectively, R_{20} for T=0.12, 0.25 and 0.50.

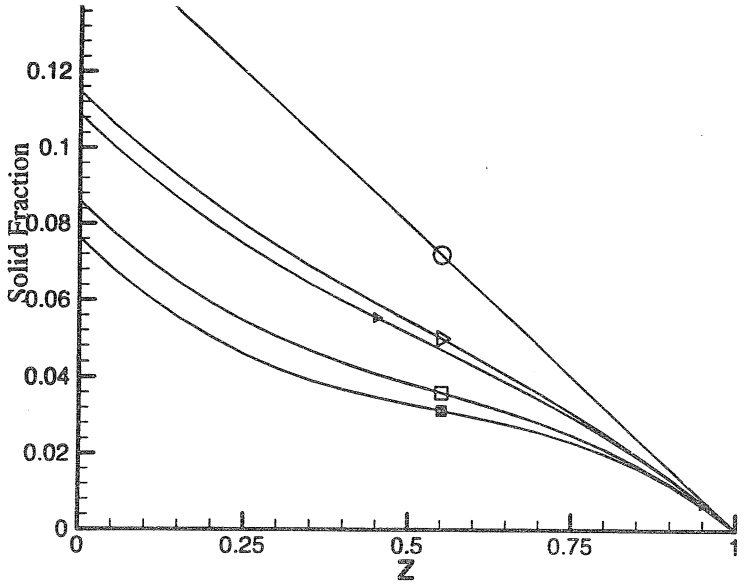

Figure 5. Solid fraction for hexagons and squares versus z for S_t=1.0, C=1.0, K_c=0.0, K_2 =0.0 and x =y =0.0. Here graph labeled by the symbol of circle presents ϕ_B, graphs labeled by the symbols of triangle and filled triangle present, respectively, $\tilde{\phi}$ for hexagons at T=0.0 and 0.50, and graphs labeled by the symbols of square and filled square present, respectively $\tilde{\phi}$ for squares at T=0.0 and 0.50.

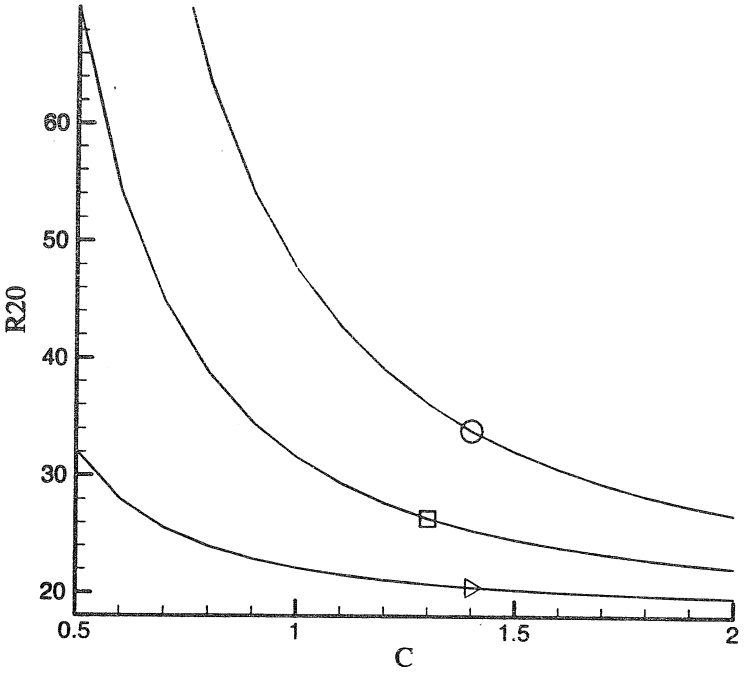

Figure 6. R_{20} against C for squares. Here S_t=1.0 and K_2=0.0. The graphs labeled by the symbols of triangle, squares and circle present, respectively, R_{20} for T=0.12, 0.25 and 0.50.

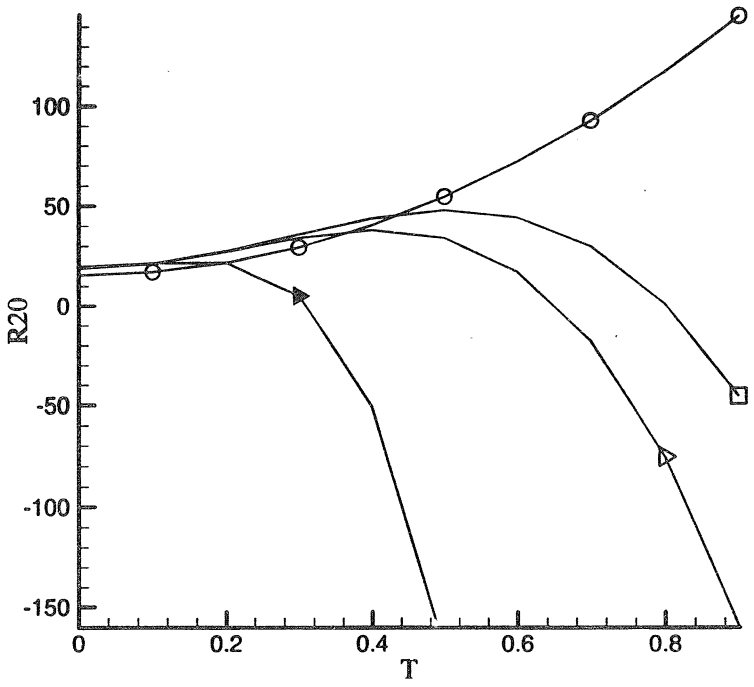

Figure 7. R_{20} against T for rolls, squares and rectangles. Here S_t=1.0, C=1.0 and K_2 =0.0. The graphs labeled by the symbols of circle, square, triangle and filled triangle present, respectively, R_{20} for rolls, squares, rectangles with γ=78.5° and rectangles with γ =66.5°.

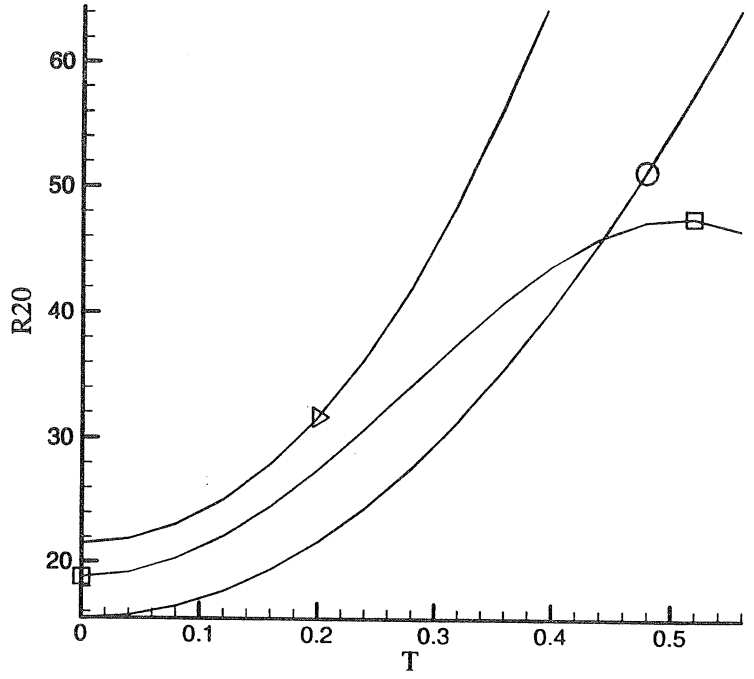

Figure 8. R_{20} against T for rolls, squares and hexagons. Here S_t=1.0, C=1.0 and K_2=0.0. The graphs labeled by the symbols of circle, square and triangle present, respectively, R_{20} for rolls, squares and hexagons.

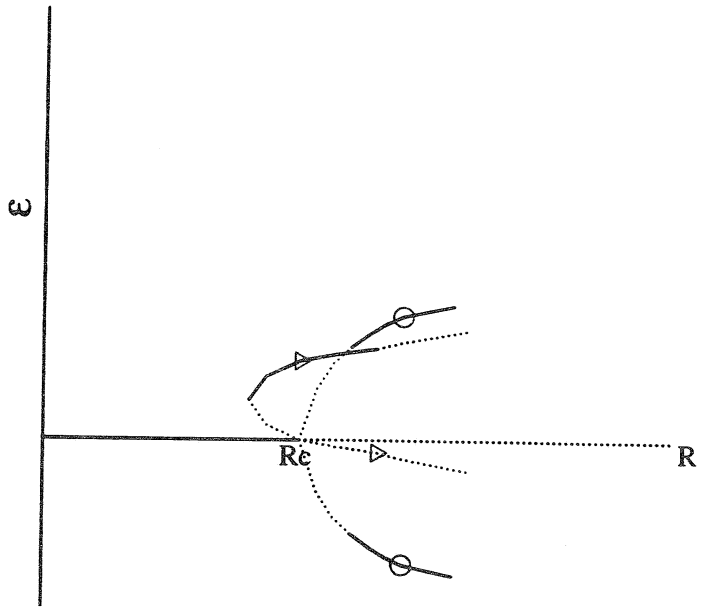

Figure 9. Bifurcation diagram in (R, ε)-plane. Here solid and dotted lines present, respectively, stable and unstable branches. The lines labeled by the symbols of triangle and circle present, respectively, hexagons and non-hexagonal cases.

List of Recent TAM Reports

No.	Authors	Title	Date
918	Riahi, D. N.	Effects of a vertical magnetic field on chimney convection in a mushy layer—*Journal of Crystal Growth* **216**, 501–511 (2000)	Aug. 1999
919	Riahi, D. N.	Boundary mode–vortex interaction in turbulent channel flow over a non-wavy rough wall—*Proceedings of the Royal Society of London A* **457**, 2643–2666 (2001)	Sept. 1999
920	Block, G. I., J. G. Harris, and T. Hayat	Measurement models for ultrasonic nondestructive evaluation—*IEEE Transactions on Ultrasonics, Ferroelectrics, and Frequency Control* **47**, 604–611 (2000)	Sept. 1999
921	Zhang, S., and K. J. Hsia	Modeling the fracture of a sandwich structure due to cavitation in a ductile adhesive layer—*Journal of Applied Mechanics* **68**, 93–100 (2001)	Sept. 1999
922	Nimmagadda, P. B. R., and P. Sofronis	Leading order asymptotics at sharp fiber corners in creeping-matrix composite materials	Oct. 1999
923	Yoo, S., and D. N. Riahi	Effects of a moving wavy boundary on channel flow instabilities—*Theoretical and Computational Fluid Dynamics* (submitted)	Nov. 1999
924	Adrian, R. J., C. D. Meinhart, and C. D. Tomkins	Vortex organization in the outer region of the turbulent boundary layer—*Journal of Fluid Mechanics* **422**, 1–53 (2000)	Nov. 1999
925	Riahi, D. N., and A. T. Hsui	Finite amplitude thermal convection with variable gravity—*International Journal of Mathematics and Mathematical Sciences* **25**, 153–165 (2001)	Dec. 1999
926	Kwok, W. Y., R. D. Moser, and J. Jiménez	A critical evaluation of the resolution properties of *B*-spline and compact finite difference methods—*Journal of Computational Physics* (submitted)	Feb. 2000
927	Ferry, J. P., and S. Balachandar	A fast Eulerian method for two-phase flow—*International Journal of Multiphase Flow*, in press (2000)	Feb. 2000
928	Thoroddsen, S. T., and K. Takehara	The coalescence–cascade of a drop—*Physics of Fluids* **12**, 1257–1265 (2000)	Feb. 2000
929	Liu, Z.-C., R. J. Adrian, and T. J. Hanratty	Large-scale modes of turbulent channel flow: Transport and structure—*Journal of Fluid Mechanics* **448**, 53–80 (2001)	Feb. 2000
930	Borodai, S. G., and R. D. Moser	The numerical decomposition of turbulent fluctuations in a compressible boundary layer—*Theoretical and Computational Fluid Dynamics* (submitted)	Mar. 2000
931	Balachandar, S., and F. M. Najjar	Optimal two-dimensional models for wake flows—*Physics of Fluids*, in press (2000)	Mar. 2000
932	Yoon, H. S., K. V. Sharp, D. F. Hill, R. J. Adrian, S. Balachandar, M. Y. Ha, and K. Kar	Integrated experimental and computational approach to simulation of flow in a stirred tank—*Chemical Engineering Sciences* **56**, 6635–6649 (2001)	Mar. 2000
933	Sakakibara, J., Hishida, K., and W. R. C. Phillips	On the vortical structure in a plane impinging jet—*Journal of Fluid Mechanics* **434**, 273–300 (2001)	Apr. 2000
934	Phillips, W. R. C.	Eulerian space–time correlations in turbulent shear flows—*Physics of Fluids* **12**, 2056–2064 (2000)	Apr. 2000
935	Hsui, A. T., and D. N. Riahi	Onset of thermal–chemical convection with crystallization within a binary fluid and its geological implications—*Geochemistry, Geophysics, Geosystems* **2**, 2000GC000075 (2001)	Apr. 2000
936	Cermelli, P., E. Fried, and S. Sellers	Configurational stress, yield, and flow in rate-independent plasticity—*Proceedings of the Royal Society of London A* **457**, 1447–1467 (2001)	Apr. 2000
937	Adrian, R. J., C. Meneveau, R. D. Moser, and J. J. Riley	Final report on 'Turbulence Measurements for Large-Eddy Simulation' workshop	Apr. 2000
938	Bagchi, P., and S. Balachandar	Linearly varying ambient flow past a sphere at finite Reynolds number—Part 1: Wake structure and forces in steady straining flow	Apr. 2000

No.	Authors	Title	Date
939	Gioia, G., A. DeSimone, M. Ortiz, and A. M. Cuitiño	Folding energetics in thin-film diaphragms—*Proceedings of the Royal Society of London A*, in press (2001)	Apr. 2000
940	Chaïeb, S., and G. H. McKinley	Mixing immiscible fluids: Drainage induced cusp formation	May 2000
941	Thoroddsen, S. T., and A. Q. Shen	Granular jets—*Physics of Fluids* **13**, 4–6 (2001)	May 2000
942	Riahi, D. N.	Non-axisymmetric chimney convection in a mushy layer under a high-gravity environment—In *Centrifugal Materials Processing* (L. L. Regel and W. R. Wilcox, eds.), 295–302 (2001)	May 2000
943	Christensen, K. T., S. M. Soloff, and R. J. Adrian	PIV Sleuth: Integrated particle image velocimetry interrogation/validation software	May 2000
944	Wang, J., N. R. Sottos, and R. L. Weaver	Laser induced thin film spallation—*Experimental Mechanics* (submitted)	May 2000
945	Riahi, D. N.	Magnetohydrodynamic effects in high gravity convection during alloy solidification—In *Centrifugal Materials Processing* (L. L. Regel and W. R. Wilcox, eds.), 317–324 (2001)	June 2000
946	Gioia, G., Y. Wang, and A. M. Cuitiño	The energetics of heterogeneous deformation in open-cell solid foams—*Proceedings of the Royal Society of London A* **457**, 1079–1096 (2001)	June 2000
947	Kessler, M. R., and S. R. White	Self-activated healing of delamination damage in woven composites—*Composites A: Applied Science and Manufacturing* **32**, 683–699 (2001)	June 2000
948	Phillips, W. R. C.	On the pseudomomentum and generalized Stokes drift in a spectrum of rotational waves—*Journal of Fluid Mechanics* **430**, 209–229 (2001)	July 2000
949	Hsui, A. T., and D. N. Riahi	Does the Earth's nonuniform gravitational field affect its mantle convection?—*Physics of the Earth and Planetary Interiors* (submitted)	July 2000
950	Phillips, J. W.	Abstract Book, 20th International Congress of Theoretical and Applied Mechanics (27 August – 2 September, 2000, Chicago)	July 2000
951	Vainchtein, D. L., and H. Aref	Morphological transition in compressible foam—*Physics of Fluids* **13**, 2152–2160 (2001)	July 2000
952	Chaïeb, S., E. Sato-Matsuo, and T. Tanaka	Shrinking-induced instabilities in gels	July 2000
953	Riahi, D. N., and A. T. Hsui	A theoretical investigation of high Rayleigh number convection in a nonuniform gravitational field—*Acta Mechanica* (submitted)	Aug. 2000
954	Riahi, D. N.	Effects of centrifugal and Coriolis forces on a hydromagnetic chimney convection in a mushy layer—*Journal of Crystal Growth* **226**, 393–405 (2001)	Aug. 2000
955	Fried, E.	An elementary molecular-statistical basis for the Mooney and Rivlin–Saunders theories of rubber-elasticity—*Journal of the Mechanics and Physics of Solids* **50**, 571–582 (2002)	Sept. 2000
956	Phillips, W. R. C.	On an instability to Langmuir circulations and the role of Prandtl and Richardson numbers—*Journal of Fluid Mechanics* **442**, 335–358 (2001)	Sept. 2000
957	Chaïeb, S., and J. Sutin	Growth of myelin figures made of water soluble surfactant—Proceedings of the 1st Annual International IEEE–EMBS Conference on Microtechnologies in Medicine and Biology (October 2000, Lyon, France), 345–348	Oct. 2000
958	Christensen, K. T., and R. J. Adrian	Statistical evidence of hairpin vortex packets in wall turbulence—*Journal of Fluid Mechanics* **431**, 433–443 (2001)	Oct. 2000
959	Kuznetsov, I. R., and D. S. Stewart	Modeling the thermal expansion boundary layer during the combustion of energetic materials—*Combustion and Flame*, in press (2001)	Oct. 2000

List of Recent TAM Reports (cont'd)

No.	Authors	Title	Date
960	Zhang, S., K. J. Hsia, and A. J. Pearlstein	Potential flow model of cavitation-induced interfacial fracture in a confined ductile layer—*Journal of the Mechanics and Physics of Solids*, in press (2002)	Nov. 2000
961	Sharp, K. V., R. J. Adrian, J. G. Santiago, and J. I. Molho	Liquid flows in microchannels—Chapter 6 of *CRC Handbook of MEMS* (M. Gad-el-Hak, ed.) (2001)	Nov. 2000
962	Harris, J. G.	Rayleigh wave propagation in curved waveguides—*Wave Motion*, in press (2001)	Jan. 2001
963	Dong, F., A. T. Hsui, and D. N. Riahi	A stability analysis and some numerical computations for thermal convection with a variable buoyancy factor—*Journal of Theoretical and Applied Mechanics*, in press (2002)	Jan. 2001
964	Phillips, W. R. C.	Langmuir circulations beneath growing or decaying surface waves—*Journal of Fluid Mechanics* (submitted)	Jan. 2001
965	Bdzil, J. B., D. S. Stewart, and T. L. Jackson	Program burn algorithms based on detonation shock dynamics—*Journal of Computational Physics* (submitted)	Jan. 2001
966	Bagchi, P., and S. Balachandar	Linearly varying ambient flow past a sphere at finite Reynolds number: Part 2—Equation of motion—*Journal of Fluid Mechanics* (submitted)	Feb. 2001
967	Cermelli, P., and E. Fried	The evolution equation for a disclination in a nematic fluid—*Proceedings of the Royal Society A* **458**, 1–20 (2002)	Apr. 2001
968	Riahi, D. N.	Effects of rotation on convection in a porous layer during alloy solidification—Chapter in *Transport Phenomena in Porous Media* (D. B. Ingham and I. Pop, eds.), Oxford: Elsevier Science (2001)	Apr. 2001
969	Damljanovic, V., and R. L. Weaver	Elastic waves in cylindrical waveguides of arbitrary cross section—*Journal of Sound and Vibration* (submitted)	May 2001
970	Gioia, G., and A. M. Cuitiño	Two-phase densification of cohesive granular aggregates	May 2001
971	Subramanian, S. J., and P. Sofronis	Calculation of a constitutive potential for isostatic powder compaction—*International Journal of Mechanical Sciences* (submitted)	June 2001
972	Sofronis, P., and I. M. Robertson	Atomistic scale experimental observations and micromechanical/continuum models for the effect of hydrogen on the mechanical behavior of metals—*Philosophical Magazine* (submitted)	June 2001
973	Pushkin, D. O., and H. Aref	Self-similarity theory of stationary coagulation—*Physics of Fluids* **14**, 694–703 (2002)	July 2001
974	Lian, L., and N. R. Sottos	Stress effects in ferroelectric thin films—*Journal of the Mechanics and Physics of Solids* (submitted)	Aug. 2001
975	Fried, E., and R. E. Todres	Prediction of disclinations in nematic elastomers—*Proceedings of the National Academy of Sciences* **98**, 14773–14777 (2001)	Aug. 2001
976	Fried, E., and V. A. Korchagin	Striping of nematic elastomers—*International Journal of Solids and Structures*, in press (2002)	Aug. 2001
977	Riahi, D. N.	On nonlinear convection in mushy layers: Part I. Oscillatory modes of convection—*Journal of Fluid Mechanics* (submitted)	Sept. 2001
978	Sofronis, P., I. M. Robertson, Y. Liang, D. F. Teter, and N. Aravas	Recent advances in the study of hydrogen embrittlement at the University of Illinois—Invited paper, Hydrogen–Corrosion Deformation Interactions (Sept. 16–21, 2001, Jackson Lake Lodge, Wyo.)	Sept. 2001
979	Fried, E., M. E. Gurtin, and K. Hutter	A void-based description of compaction and segregation in flowing granular materials—*Proceedings of the Royal Society of London A* (submitted)	Sept. 2001
980	Adrian, R. J., S. Balachandar, and Z.-C. Liu	Spanwise growth of vortex structure in wall turbulence—*Korean Society of Mechanical Engineers International Journal* **15**, 1741–1749 (2001)	Sept. 2001

No.	Authors	Title	Date
981	Adrian, R. J.	Information and the study of turbulence and complex flow—*Japanese Society of Mechanical Engineers Journal B*, in press (2002)	Oct. 2001
982	Adrian, R. J., and Z.-C. Liu	Observation of vortex packets in direct numerical simulation of fully turbulent channel flow—*Journal of Visualization*, in press (2002)	Oct. 2001
983	Fried, E., and R. E. Todres	Disclinated states in nematic elastomers—*Journal of the Mechanics and Physics of Solids*, in press (2002)	Oct. 2001
984	Stewart, D. S.	Towards the miniaturization of explosive technology—Proceedings of the 23rd International Conference on Shock Waves (2001)	Oct. 2001
985	Kasimov, A. R., and Stewart, D. S.	Spinning instability of gaseous detonations—*Journal of Fluid Mechanics* (submitted)	Oct. 2001
986	Brown, E. N., N. R. Sottos, and S. R. White	Fracture testing of a self-healing polymer composite—*Experimental Mechanics* (submitted)	Nov. 2001
987	Phillips, W. R. C.	Langmuir circulations—*Surface Waves* (J. C. R. Hunt and S. Sajjadi, eds.), in press (2002)	Nov. 2001
988	Gioia, G., and F. A. Bombardelli	Scaling and similarity in rough channel flows—*Physical Review Letters* **88**, 014501 (2002)	Nov. 2001
989	Riahi, D. N.	On stationary and oscillatory modes of flow instabilities in a rotating porous layer during alloy solidification—*Journal of Porous Media* (submitted)	Nov. 2001
990	Okhuysen, B. S., and D. N. Riahi	Effect of Coriolis force on instabilities of liquid and mushy regions during alloy solidification—*Physics of Fluids* (submitted)	Dec. 2001
991	Christensen, K. T., and R. J. Adrian	Measurement of instantaneous Eulerian acceleration fields by particle-image accelerometry: Method and accuracy—*Experimental Fluids* (submitted)	Dec. 2001
992	Liu, M., and K. J. Hsia	Interfacial cracks between piezoelectric and elastic materials under in-plane electric loading—*Journal of the Mechanics and Physics of Solids* (submitted)	Dec. 2001
993	Panat, R. P., S. Zhang, and K. J. Hsia	Bond coat surface rumpling in thermal barrier coatings—*Acta Materialia* (submitted)	Jan. 2002
994	Aref, H.	A transformation of the point vortex equations—*Physics of Fluids* (submitted)	Jan. 2002
995	Saif, M. T. A, S. Zhang, A. Haque, and K. J. Hsia	Effect of native Al_2O_3 on the elastic response of nanoscale aluminum films—*Acta Materialia* (submitted)	Jan. 2002
996	Fried, E., and M. E. Gurtin	A nonequilibrium theory of epitaxial growth that accounts for surface stress and surface diffusion—*Journal of the Mechanics and Physics of Solids* (submitted)	Jan. 2002
997	Aref, H.	The development of chaotic advection—*Physics of Fluids* **14**, 1315–1325 (2002); see also *Virtual Journal of Nanoscale Science and Technology*, 11 March 2002	Jan. 2002
998	Christensen, K. T., and R. J. Adrian	The velocity and acceleration signatures of small-scale vortices in turbulent channel flow—*Journal of Turbulence*, in press (2002)	Jan. 2002
999	Riahi, D. N.	Flow instabilities in a horizontal dendrite layer rotating about an inclined axis—*Proceedings of the Royal Society of London A* (submitted)	Feb. 2002
1000	Kessler, M. R., and S. R. White	Cure kinetics of ring-opening metathesis polymerization of dicyclopentadiene—*Journal of Polymer Science A* (submitted)	Feb. 2002
1001	Dolbow, J. E., E. Fried, and Amy Q. Shen	Point defects in nematic gels: The case for hedgehogs—*Proceedings of the National Academy of Sciences* (submitted)	Feb. 2002
1002	Riahi, D. N.	Nonlinear steady convection in rotating mushy layers—*Journal of Fluid Mechanics* (submitted)	Mar. 2002